Wisconsin
Indiana
Yale
Noao

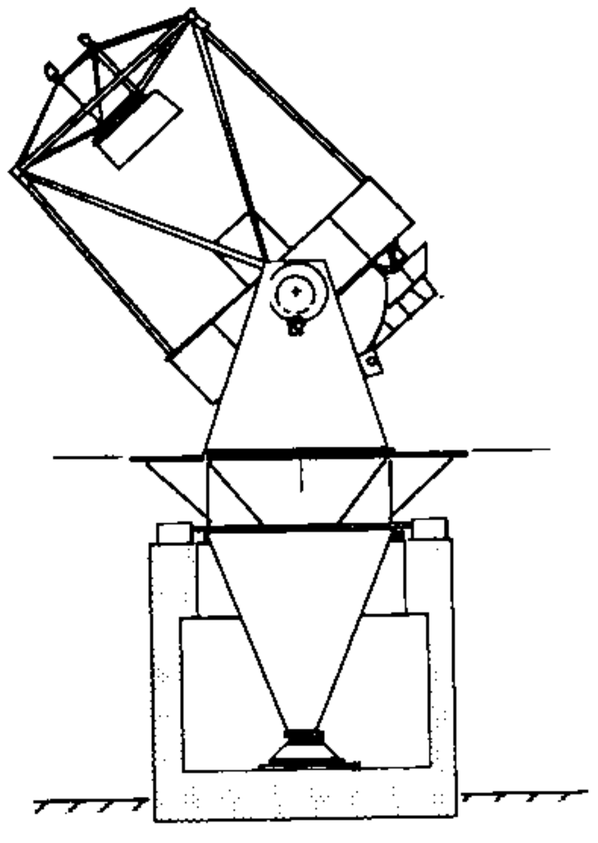

3.5 Meter Telescope

# Engineering Report
# Preliminary Design Study
# WIYN 3.5 Meter Telescope

**WODC 02-03-01**

June 1990

# ENGINEERING REPORT - PRELIMINARY DESIGN STUDY

# WISCONSIN-INDIANA-YALE-NOAO (WIYN) 3.5 METER TELESCOPE

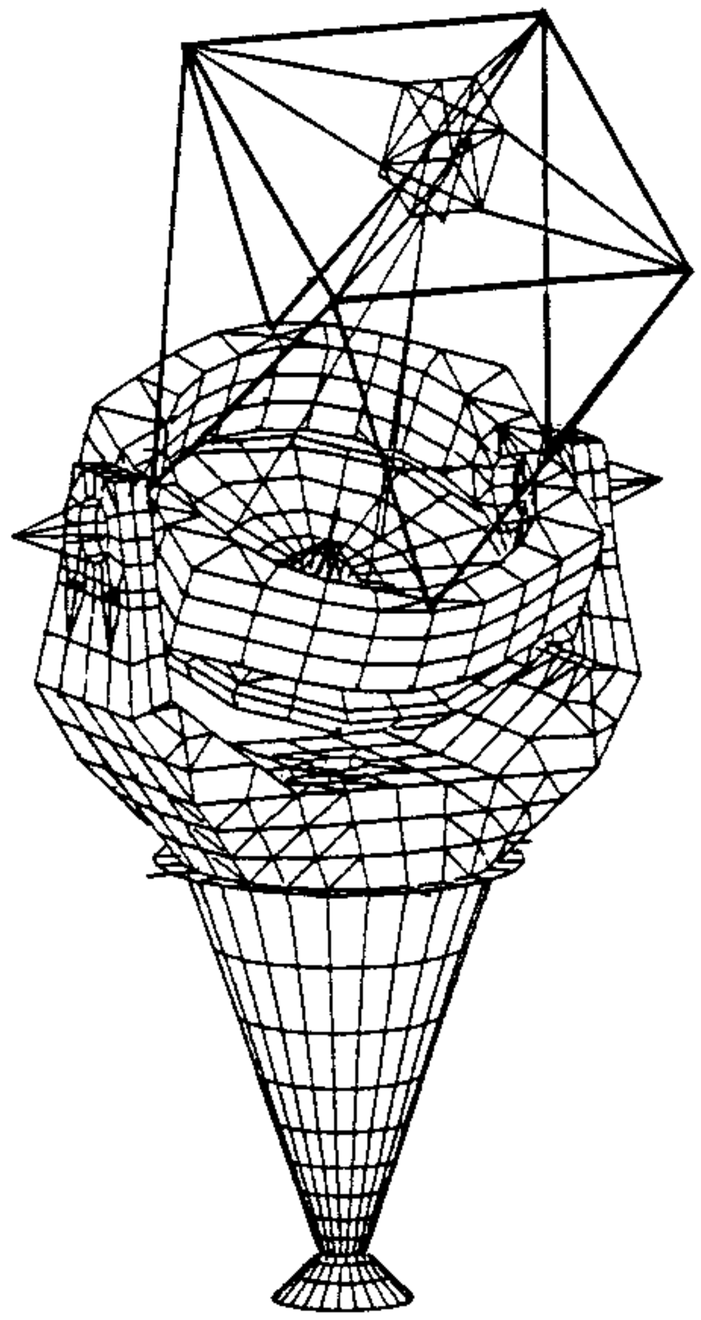

for


**NATIONAL OPTICAL ASTRONOMY OBSERVATORIES**

P. O. Box 26732
950 N. Cherry Ave.
Tucson, Arizona 85726-6732

by

**L & F INDUSTRIES**

P. O. Box 40
2110 Belgrave Ave.
Huntington Park, Ca. 90255



June 1990

# INDEX

# 1.0 INTRODUCTION

This report summarizes a preliminary design study of the Wisconsin-Indiana-Yale-NOAO (WIYN) 3.5 Meter Telescope performed for NOAO by L & F Industries. The purpose of the study has been to determine what structural and mechanical changes might be required from the recently constructed Apache Point Observatory (APO) 3.5 Meter Telescope, used as an initial baseline for the study. The objectives of the report have been to define the telescope design and summarize its expected performance.

To these ends, considerable finite element analysis has been performed both on the Optics Support Structure (OSS), to predict optical misalignments due to rotating through the gravity field, and on the entire telescope to predict wind effects and modal performance for the structure.

Data reductions and current layout drawings are included in the appendix.

# 2.0 STRUCTURAL AND MECHANICAL CONFIGURATION

## 2.1 SYSTEM DESCRIPTION:

The WIYN 3.5 Meter Telescope design summarized herein consists of an Alt-Azimuth Fork mount, using rolling element bearings to define the altitude axis and lower end of the azimuth axis. The upper end of the azimuth axis is defined using drive and idler rollers which are in turn supported by rolling element bearings. The system is shown on drawings E305000 (sheets 1 and 2), D305003, E305006, and E305007 (sheets 1 and 2) as well as graphics plots in Figures 1 through 16. The 3.5 meter f1.75 primary mirror and f6.3 secondary mirror focus at either of two Nasmyth instrument locations or at a third instrument location, on the OSS center section.

The two main rotating structural assemblies of the mount are the Optics Support Structure and the Fork.

The OSS Assembly (E305000 sheets 1 and 2) consists of three major subassemblies:

1.) The mirror cell assembly includes the cell structure (ref KPNO Drawing 3500.0002073E, not included in this report), the primary mirror, and its support and ventilation systems.

2.) The center section includes the center section structure, mirror cover, and altitude bearings. It also supports the altitude drive disks and primary truss.

3.) The secondary end includes the secondary main truss, square frame, vanes, secondary center structure, and secondary mirror, cell, and support system.

The Fork Assembly (E305007 sheets 1 and 2) consists of the cone, azimuth drive disk, fork weldment, pillow blocks, and altitude axles.

In addition there is a stationary lower bearing support pedestal (E307007 sheet 2 and D305003), and square frame azimuth support system, E305006.

## 2.2 STRUCTURAL DESIGN:

The structural design is intended to maximize stiffness and reduce weight, achieving relatively high modal performance without the necessity of hydrostatic bearings. High stiffness and low weight effect small deflections due to gravity and wind loading, and high structural resonant frequencies. In addition, the low weight may effect cost savings, but will certainly improve thermal response of the structure to ambient temperature changes. This will then have a beneficial effect on seeing.

As can be seen on the drawings and graphics plots herein, the telescope structure is generally constructed using plate fabrications. Plates used are predominantly 3/8" and 1/2" thick carbon steel. Notable exceptions to this are the secondary and primary end main truss members, which are made from 4 in. outside diameter x 1/2 in. wall steel tubing. All weldments are to be thermally stress relieved. Detailed descriptions of plate thicknesses and member sizes are included in the graphics plots, Figures 4 through 16.

## 2.3 BEARINGS:

Some preliminary study of various rolling element bearing types was conducted for both the altitude and azimuth axes. A detailed discussion of all configurations considered is beyond the scope of this report. However, a description of the current favored types, and reasons for these tentative selections, is provided as follows:

### 2.31 Altitude Bearings:

The moment-carrying duplex pair of angular contact ball bearings, shown on E305007 sheet 2, is preferred for the altitude bearings. The bearings tentatively selected are Kaydon KG250AR( )BR2Z, selected to .0008 in. runout. The duplex pairs would be individually preloaded (that is, each pair) sufficient to keep all clearance out of the bearing under full load of the OSS assembly. The bearing support axles will be pre-cocked to accomplish a nominally zero moment on each pair with the system fully assembled and under the influence of gravity. While these bearings may not have friction as low as spherical roller radial bearings, they are likely to have lower non-repeatable runout due to the use of more precise balls (rather than individually machined rollers). The friction can be minimized by using

a low preload and by precocking the axles. The bearings have good availability and relatively low cost.

2.32 Azimuth Bearings:

The upper end of the azimuth axis will be defined by two drive and two idler roller units, spaced at 90° around the axis. The bearings used to support these rollers, and the rollers themselves will be manufactured to minimize non-repeatable pointing errors.

The lower azimuth bearing is tentatively planned as a spherical roller thrust bearing, either SKF 29292 or FAG 29292E.MB. This bearing provides the self-alignment feature necessary for this application, has low friction, and is available at reasonable cost. A test of non-repeatable runout (or "noise") on the similar bearing used at Apache Point Observatory is planned prior to firm commitment to this bearing type. This bearing, as well as an alternate concept sketch for a self-aligning ball bearing, is shown on D305003. One other possible type here is an externally self-aligning ball bearing, although further study would be required to determine possible deleterious effects within the bearing due to the external self-alignment.

## 2.4 DRIVES:

Friction drives are planned for both telescope axes. The altitude axis will use one drive unit near the inside of each fork tine, with the drive mounted to the fork and driving against an altitude drive disk mounted to either edge of the center section of the OSS (ref E305000 sheets 1 and 2).

The azimuth axis drive concept uses two drives at 180° to each other driving against a drive disk at the top of the cone of the fork. This is shown on drawing E305006. In the case of both drives (altitude and azimuth) the drive boxes have stiff restraints only in the tangential (drive) direction. They are otherwise free to articulate except that they are guided by rollers registering against the edge of the drive disks which is perpendicular to the drive surface, and the dual preloaded-roller feature prevents rotation of the unit about an axis parallel to the rotation axis.

The drive units themselves might be designed in either of two ways. One possibility would be to use a virtual duplicate of the APO drives, which consist of a small D. C. servomotor driving the traction roller through a two-stage reducer, the reduction stages of which also use friction drive contacts. This system then provides a total reduction of about 1300:1 from the servomotor to the axis of the telescope. Another possibility would be to use a scaled-down version of the "Direct Friction Drive" being planned for the Magellan Project 8 Meter Telescope, with a total reduction of about 35:1. Both methods offer the benefits of high stiffness and low noise at relatively low cost.

# 3.0 FINITE ELEMENT ANALYSIS

## 3.1 INTRODUCTION:

The finite element models are shown in the form of graphics plots in Figures 1 through 25. Five final models were used to determine structural performance of the system, summarized in the following pages.

WINOSS1 is a model of the OSS alone with the mirror cell highly meshed and a complex system of beam elements to accurately simulate the function of the primary mirror axial and lateral support systems. Zenith and horizon gravity loading are applied and combined to determine the optical misalignments due to rotating through the gravity field. This model and its results are described in sections 3.5 and 3.6 below.

Models WIYNTZ and WIYNTH are zenith and horizon-pointing models of the complete telescope to determine wind performance. A simplified primary mirror cell was used with the primary mirror pointing referenced directly from three hard points on the cell. Front and side wind loads were applied, as described later (3.4 Wind Performance).

Models WIYNTM17 and WIYNTM18 are the final versions of the modal analysis. The former used two altitude drives, the latter a single drive on one side of the OSS. The earlier versions (WIYNTM through WIYNTM16) were run for optimization purposes. These results are reported in section 3.3, Modal Analysis. Example model sizes are:

| WIYNTM17 | | WINOSS1 | |
|---|---|---|---|
| 1608 | nodes | 1861 | nodes |
| 1986 | plate elements | 2324 | plate elements |
| 297 | beam elements | 648 | beam elements |
| 9,462 | degrees of freedom | 11,037 | degrees of freedom |
| 786 | bandwidth | 1247 | bandwidth |

## 3.2 OPTICS, INSTRUMENT, AND TELESCOPE WEIGHTS:

The following weights were used in, or resulted from, the finite element models:

Primary Mirror - 4,427 lbs.
Axial Support System - 2,856 lbs.
Lateral Support System - 278 lbs.
Nasmyth Instruments - (2) @ 1,500 lbs.
OSS Assembly - 32,660 lbs.:
5.5E5 lb-sec$^2$-in (altitude axis)
4.3E5 lb-sec$^2$-in (optical axis)
5.9E5 lb-sec$^2$-in (perpendicular)

Secondary Mirror - 357 lbs.
Secondary Mirror Cell - 250 lbs.
Tertiary Assembly - 1,571 lbs.

Telescope (rotating) Assembly:
80,000 lbs.
1.11E6 lb-sec$^2$-in (azimuth)

## 3.3 MODAL ANALYSIS:

The results of the finite element analyses are presented in Tables 1 and 2 and in the graphics plots in Figures 17 through 20. As can be seen in the left side of Figure 17, the final models were run with the OSS pointing 30° off zenith. It was felt that this was a reasonable compromise between the zenith attitude, where the lateral translation frequency would be slightly lower, and the horizon attitude, where the locked rotor azimuth frequency would be lower. It is estimated that the lateral translation frequency would be about 2% lower, and the locked rotor azimuth about 4% lower, than the results reported herein. The OSS was positioned at the 30° position since the telescope is used far more frequently near zenith than it is near horizon.

The optimizing runs that were made are summarized in Table 2. Some conclusions that can be drawn from the table are:

1. The translational modes are much more reliant on stiffness of the fork structure than on support stiffness (TM5 vs. TM7 and TM10).

2. The locked rotor azimuth mode is much more reliant on drive stiffness than it is on stiffness of the fork structure (TM5 vs. TM7 and TM10).

3. The base area of the fork offers much greater potential for improving the primary modes than the tines or cone (TM5 vs. TM6, TM8, and TM9).

4. The longer cone caused a relatively significant improvement (TM5 to TM11), presumably by making the supports more effective.

5. Only small improvements can be achieved by changing plate thicknesses in the fork structure, since mass and stiffness effects have opposite sign (TM12 through TM16).

6. A noticeable but still small improvement is caused by reducing the vertical depth of the base (TM16 vs. TM19).

From these results, it was concluded that 1.) the 20" longer cone is worthwhile since its added cost is partially or totally offset by reducing the amount of concrete required in the bottom of the pier, 2.) the upper 60% of the cone should be lighter (3/4" vs. 1") since the performance loss is negligible as compared to favorable cost and thermal effects, 3.) the base shell thickness should be 3/4", and 4.) the thinner base vertical dimension doesn't offer sufficient performance improvement to overcome its disadvantage of reduced clearance and space for maintenance operations.

Therefore, the final modal analyses, models WIYNTM17 and WIYNTM18 had the 20" longer cone, 3/4" thick upper cone, and 3/4" thick base shell. The final frequencies and modeshape descriptions for the complete telescope models are then shown in Table 1.

The modeshapes are shown and briefly discussed in Figures 17 through 20, (and on video supplied under separate cover) and will therefore not be reiterated here. A few points should be made, however.

Modeshape 4 (Figure 20) is effectively the "second mode" of modeshape 1; that is, only the phase relationship of the OSS and fork motions changes from mode 1 to mode 4. Mode 4 was assigned the name "locked rotor altitude" simply because it involves much more motion of the altitude drives. Mode 1, or "fore-aft translation" may be more critical from a controls standpoint, however, because its frequency is lower (7.3 vs. 10.6 hz.).

Modes 5 and 6 were initially at about 9 hertz and were increased by adding a local brace to stiffen them laterally.

The mode 7 frequency was calculated manually, since it is defined almost entirely by vane pretension, an effect not included in the linear static finite element program used for these solutions. The method used for the manual calculation is rather simplistic, and a more accurate estimate can be made by applying a special-purpose "load stiffening" program, such as during the detail design phase.

As can be seen by comparing the results of WIYNTM18 with WIYNTM17, the effect of eliminating one of the altitude drives is significant and adverse. As expected, both the locked rotor altitude and fore-aft translation modes were reduced to about 80% of the frequencies with two drives.

### 3.4 STATIC ANALYSIS - WIND LOADING:

Effects of wind loading on the complete telescope structure are shown in Figures 21 through 23 and in Table 3. Front and side wind loading was applied in the zenith attitude with and without the secondary baffle installed. In the horizon-pointing attitude side wind was applied with and without the secondary baffle. Under a horizon front wind the effect of the baffle is negligible.

Without the benefit of a wind tunnel test (or other more detailed analysis beyond the scope of this effort) wind pressure loading was simply applied to all members exposed to the wind. This was done as if the telescope, above the observing floor, were exposed to a free air flow velocity of 15 mph, with a 7,000 ft. elevation air density. The actual pressure loading used was 0.46 psf (pounds/ft.$^2$). From recent testing at APO this should generally be representative of about a 45 mph ambient wind remote from the enclosure.

It should be noted that elements representing both the altitude and azimuth "locked rotor" drive stiffness were used in these models, as well as in the modal analyses. The 400,000 lbs./in. spring rates are the measured tangential stiffness of the APO drives, measured at the drive roller with the servomotor rotor mechanically locked. This would, however, be very conservative in a steady wind, since the encoders will reference to the drive disks and

not the motor rotor. Therefore, in a steady wind, the drives would behave much more stiffly, and the pointing errors for such a case may be much lower than the values in Table 3.

Absolute displacements of nodes representing the optics, as well as data reductions determining the relative motions of the primary and secondary mirrors, are included in the Appendix. The primary pointing errors and optical misalignments are shown in Table 3.

### 3.5 STATIC ANALYSIS - ROTATING THROUGH THE GRAVITY FIELD:

Model WINOSS1 was created to determine optical misalignments due to rotating through the gravity field. This was done by applying zenith and horizon component gravity loads separately and combining their effects with a post-processing program. Exaggerated deflected plots of horizon and (separately) zenith gravity loading are shown in Figures 24 and 25. The absolute motions of nodes representing the optics, as well as the calculations converting these to relative motions, are in the appendix. The resulting relative motions are provided in Table 4. It should be noted that the restraints and balance of the OSS model were such that a small rotation of the model occurred (about 30 arcsec). Therefore, the absolute displacement values in the appendix table ("Gravity Displacements - WIYN Optics Support Structure") are not meaningful, but *relative* motions between nodes are.

As can be seen in Figure 24, the primary mirror moves (laterally) much more than does the primary end structure. This is due to the compliance of the primary mirror lateral support system, which was modelled as 10,000 lbs./in. per support. A detailed description of the primary mirror support system finite element model follows.

### 3.6 STATIC ANALYSIS - PRIMARY MIRROR SUPPORT SYSTEM:

Figures 9 and 11 show the portion of WINOSS1 representing the primary mirror, cell, and support system. As can be seen in Figure 9, a highly meshed plate element model of the cell was required to interface with the support system model. The complex mesh of the cell plus effectively simulating the hydraulic load sharing of the mirror support system made for a challenging and complex model.

Three of the mirror's six degrees of freedom are defined by the axial support system: piston and the two tilts. This is accomplished in the real system by three zones of hydraulic pistons which are interconnected within each zone. There are 22 hydraulic supports in each zone. Therefore, as the structure deflects (especially due to the zenith gravity component), each of the three zones in the hydraulic system averages the complex distorted shape of the back plate of the mirror cell. The back plate is applicable here, since the axial supports mount to the back plate of the cell and connect to the back plate of the mirror by long pushrods through the cell structure.

It was determined that springs could be used to "withdraw motion" from a "sector model" in the same way that the real hydraulic piston withdraws oil from the other 21 pistons (within its axial support zone). That is, if the real mirror were sitting on the real support system and the structure under only one piston were to be lowered locally, that zone would lower, on average, a much smaller amount and cause a pointing of the mirror. Likewise, if the cell is connected to the "sector" model (a rigid, weightless set of plate elements in plane with the back plate of the mirror) by a series of 22 very soft springs, then when the bottom of one spring is lowered, a force will develop which must be reacted by all 21 of the other soft springs, and the average, or centroid, of the sector lowers a much smaller amount. If this is true for the lowering of one point on the cell, then it must be true for the lowering of any of the points on the cell, and therefore holds true for any complex shape that the cell might take. The accuracy of this method was verified by local finite element modelling.

The lower left area of Figure 11 indicates the axial support system model. The three sections of plate elements are the "sector models", and are rigid and weightless. They are connected to the back plate of the cell by 22 axial beam elements per sector. Actually, each axial beam element is two elements; a long compliant one in series with a short relatively stiff one that subsequently attaches to the back plate of the cell. The short elements perpendicular to the axial elements are for local stiffening of the cell back plate by the real axial support "box". The weight of the mirror (actually, zenith gravity component load for each axial support) is applied to the top of the short axial beam, so that its axial strain simulates the motion caused by the spring rate of the axial supports in the real system (24,000 lbs./in.). The cross-sectional areas of the soft springs, although small, are proportioned with respect to each other so that they correctly represent the various hydraulic areas of the real axial supports. They are compliant enough, however, that the final load in them (due to the final distorted shape of the back plate of the cell) is sufficiently small that they have a negligible effect on the cell shape.

With this simulation, although the "sector models" tilt locally, their centroids end up at the correct height above the cell. Therefore, if the primary mirror ties to them in such a way that their tilts don't affect the mirror pointing, they accurately serve their purpose of determining those three degrees of freedom of the primary mirror. An important characteristic of this portion of the model is that the mirror weight does *not* go through the support system in the model, but only through the short series beam with the proper axial support system spring rate.

The next group of elements exploded above the axial support system in Figure 11 represents the 24 lateral support units but does not include the hydraulic sharing feature of the lateral support system. Each unit in the finite element model consists of four short, rigid beam elements in the plane of the front plate of the cell, plus a short perpendicular element. The perpendicular element is rigid except that its shear compliance is sized for the correct spring rate of the real lateral support unit (10,000 lbs./in.). Therefore, like in the axial support system model, the (horizon) gravity

component loading is applied at the end of the short, relatively stiff beam and does not go through the soft springs used for hydraulic sharing, described below.

This next set of beam elements simulates the hydraulic sharing for the lateral support system in an analagous fashion to that of the axial supports described above. The parallel lines in the view in Figure 11 are actually a series of overlapping soft beam elements which connect each axial support unit to the primary mirror.

Finally, the upper right group in Figure 11 represents the primary mirror and the "collimation links" at the upper left and lower right areas of that view. The rigid, weightless beam elements are used to connect the lateral support system hydraulic sharing elements (one degree of freedom), plus the centroids of the three "sector models" (three degrees of freedom), the two collimation links (two degrees of freedom), and node 1392, the primary mirror axis at the secondary vertex.

In summary, the final loading seen by the finite element model (FEM) of the mirror cell is the same as for the real cell, since it is applied as a series of (66 plus 24) nodal loads, at the proper locations. These loads are applied through relatively rigid springs representing the true spring rates of the axial support system. Therefore, the distorted shape of the cell, including the axial and lateral supports, is accurate. The soft springs that then connect between those points and the model of the primary mirror accurately simulate the hydraulic sharing of the support systems. The rigid, weightless primary mirror model must then have the same motion relative to the FEM cell as the real mirror has relative to the real cell.

## 4.0 SUMMARY AND CONCLUSIONS

The preliminary design has been defined, and gravity, wind, and modal performance predicted, for the WIYN 3.5 Meter Telescope. No optimizing has been performed within the OSS, although some effort has been made to improve the primary mode frequencies by optimizing of the fork structure. "Locked rotor" performance would be improved by stiffer drives, such as a scaled-down Magellan Project direct friction drive. It can also be argued, however, that a high performance drive effectively simulates infinite drive stiffness, and that therefore "locked encoder" or "controlled rotor" modes should be used to predict modal and wind performance. These effects, more extensive optimizing, verification of some of the assumptions made in these models, and analysis of secondary end local modes using vane pretension, are possible areas for study during the detail design phase.

## FINITE ELEMENT ANALYSIS - SUMMARY OF RESULTS

### TABLE 1
### NATURAL FREQUENCIES AND MODESHAPES

The following modal performance is from model WIYNTM17, which assumes two altitude drives (one at each edge of the OSS). The four primary modeshapes are shown in Figures 17 through 20. Additional discussion can be found in the body of the report.

| MODE | FREQUENCY hertz | MODESHAPE DESCRIPTION |
|---|---|---|
| 1 | 7.3 | Fore-Aft Translation |
| 2 | 7.6 | Lateral Translation |
| 3 | 8.8 | Locked Rotor Azimuth Axis |
| 4 | 10.6 | Locked Rotor Altitude Axis |
| 5 | 14.7 | Altitude Disks Out-of-plane Bending |
| 6 | 14.7 | Orthogonal of Mode 5 |
| 7 | 16.4 | Secondary Assembly Rotation about the Optical Axis (manual calculation) |
| 8 | 18.6 | Main Truss Tube Bending (local mode) |

The following performance is from model WIYNTM18, which uses only one altitude drive (at one edge of the OSS).

| MODE | FREQUENCY hertz | MODESHAPE DESCRIPTION |
|---|---|---|
| 1 | 5.7 | Fore-Aft Translation |
| 2 | 7.6 | Lateral Translation |
| 3 | 8.7 | Locked Rotor Azimuth Axis |
| 4 | 9.2 | Locked Rotor Altitude Axis |
| 5 | 13.6 | Altitude Disk Out-of-plane Bending |
| 6 | 14.7 | Orthogonal of mode 5 |
| 7 | 16.4 | Secondary Assembly Rotation about the Optical Axis (manual calculation) |
| 8 | 18.5 | Main Truss Tube Bending (local mode) |

## TABLE 2
## MODAL OPTIMIZATION

The modal optimization began with complete models of the telescope, models WIYNTM through WIYNTM4. Since it became apparent that the detailed OSS portion of the model was serving little purpose (the optimizing of the primary modes is much more effectively done in the fork), the OSS structure was replaced, beginning with WIYNTM5, by two point masses, one at each altitude axle. In this way, the optimizing proceeded much faster. When the final changes were decided upon, they were then made to the complete telescope model and run. This final version was model WIYNTM17. A summary follows:

| MODEL | DESCRIPTION | LATERAL | FORE-AFT | LRAZ |
|---|---|---|---|---|
| WIYNTM5 | 2-point OSS; new baseline | 7.1 | 8.2 | 8.3 |
| WIYNTM7 | • stiff supports and az drives | 10.1 | 14.1 | 16.6 |
| WIYNTM10 | • stiff (entire) structure | 21.6 | 18.9 | 11.3 |
| WIYNTM6 | • tines (including pillow blocks) | 7.8 | 8.6 | 8.7 |
| WIYNTM8 | • base ("throat" of fork) | 11.1 | 12.2 | 10.4 |
| WIYNTM9 | • cone | 7.6 | 8.7 | 8.4 |
| WIYNTM11 | TM5 but 20" longer cone | 7.46 | 8.60 | 8.24 |
| WIYNTM12 | TM11 but 3/4" thick cone | 7.33 | 8.47 | 8.23 |
| WIYNTM13 | TM12 but lwr 40% of cone 1" thick | 7.41 | 8.56 | 8.25 |
| WIYNTM14 | TM11 but base shell ½" → ¾" | 7.63 | 8.68 | 8.28 |
| WIYNTM15 | TM11 but all plates in base 3/4" | 7.73 | 8.71 | 8.27 |
| WIYNTM16 | TM13 but base shell 3/4" | 7.57 | 8.63 | 8.29 |
| WIYNTM19 | TM16 but 37" base to 27" deep | 7.69 | 8.93 | 8.26 |

The final modal analysis, WIYNTM17, was based upon WIYNTM16; with 3/4" thick base shell, 1" lower cone, and 20" longer cone.

## TABLE 3
## WIND LOAD DEFLECTIONS

The following data are from models WIYNTZ and WIYNTH (and data reductions made from these results) and are based upon a 15 mph wind *acting upon the telescope structure.* It is expected that this is generally representative of a 45 mph ambient wind remote from the enclosure. Graphics plots of the deflected structure are provided in Figures 21 through 23. Additional discussion can be found in the body of the report.

| Attitude/Wind Direction | Primary Pointing Error | Secondary Misalignment Decenter | Rotation |
|---|---|---|---|
| zenith/front wind (no secondary baffle) | .76 arcsec | 8.6E-5 in. 2.2 microns | .017 arcsec |
| zenith/front wind (with baffle) | .85 arcsec | 1.5E-4 in. 3.8 microns | .4 arcsec |
| zenith/side wind (no baffle) | .21 arcsec | 8E-5 in. 2 microns | .02 arcsec |
| zenith/side wind (with baffle) | .23 arcsec | 1.52E-4 in. 3.9 microns | .58 arcsec |
| horizon/front wind (baffle negligible) | .46 arcsec | 7.15E-5 in. 1.8 microns | .16 arcsec |
| horizon/side wind (no baffle) | .28 arcsec | 7.4E-5 in. 1.9 microns | .03 arcsec |
| horizon/side wind (with baffle) | .32 arcsec | 1.45E-4 in. 3.7 microns | .59 arcsec |

## FINITE ELEMENT ANALYSIS - SUMMARY OF RESULTS
(Continued)

### TABLE 4
### GRAVITY MISALIGNMENTS

The following results are from model WINOSS1. If optics are perfectly aligned at zenith, these misalignments will develop between the secondary and primary mirrors (primary on passive support system) as the OSS is rotated to horizon. Motions are referenced to the secondary mirror vertex.

| NET DESPACE (PISTON) | NET Y-DECENTER (SAG) | NET X-DECENTER | NET TILT (ROTATION) |
|---|---|---|---|
| .0022 in.*<br>56 microns | .0037 in.**<br>94 microns | .00036 in.<br>9 microns | 29 arcsec*** |

If optics are perfectly aligned at zenith the following misalignments will develop between the secondary and primary mirrors (primary support actively controlled to hold fixed height off cell of primary at three reference points) as the OSS is rotated to horizon.

| NET DESPACE (PISTON) | NET Y-DECENTER (SAG) | NET X-DECENTER | NET TILT (ROTATION) |
|---|---|---|---|
| .0032 in.*<br>81 microns | .0217 in.~<br>550 microns | (zero) | 19 arcsec*** |

If optics are perfectly aligned at zenith the following misalignments will develop between the tertiary mirror and primary mirror axis (primary on passive support system) as the OSS is rotated to horizon.

| Y-DECENTER (SAG) | X-DECENTER |
|---|---|
| .0165 in.^<br>419 microns | .00021 in.<br>5 microns |

## FINITE ELEMENT ANALYSIS - SUMMARY OF RESULTS
(Continued)

### TABLE 4
### GRAVITY MISALIGNMENTS
(Continued)

If optics are perfectly aligned at zenith the following misalignments will develop between the tertiary mirror and primary mirror axis (primary support actively controlled to hold fixed height off cell of primary at three reference points) as the OSS is rotated to horizon.

| Y-DECENTER (SAG) | X-DECENTER |
|---|---|
| .0020 in. ^ ^<br>51 microns | 1E-6 in.<br>.03 microns |

If optics are perfectly aligned at zenith the tertiary will drop .0065 in. (165 microns) below the altitude axis as the OSS is rotated to horizon.

* separation

** primary axis below secondary vertex

*** secondary mirror angled down back toward primary

~ primary axis above secondary vertex

^ primary axis below tertiary

^ ^ tertiary below primary axis

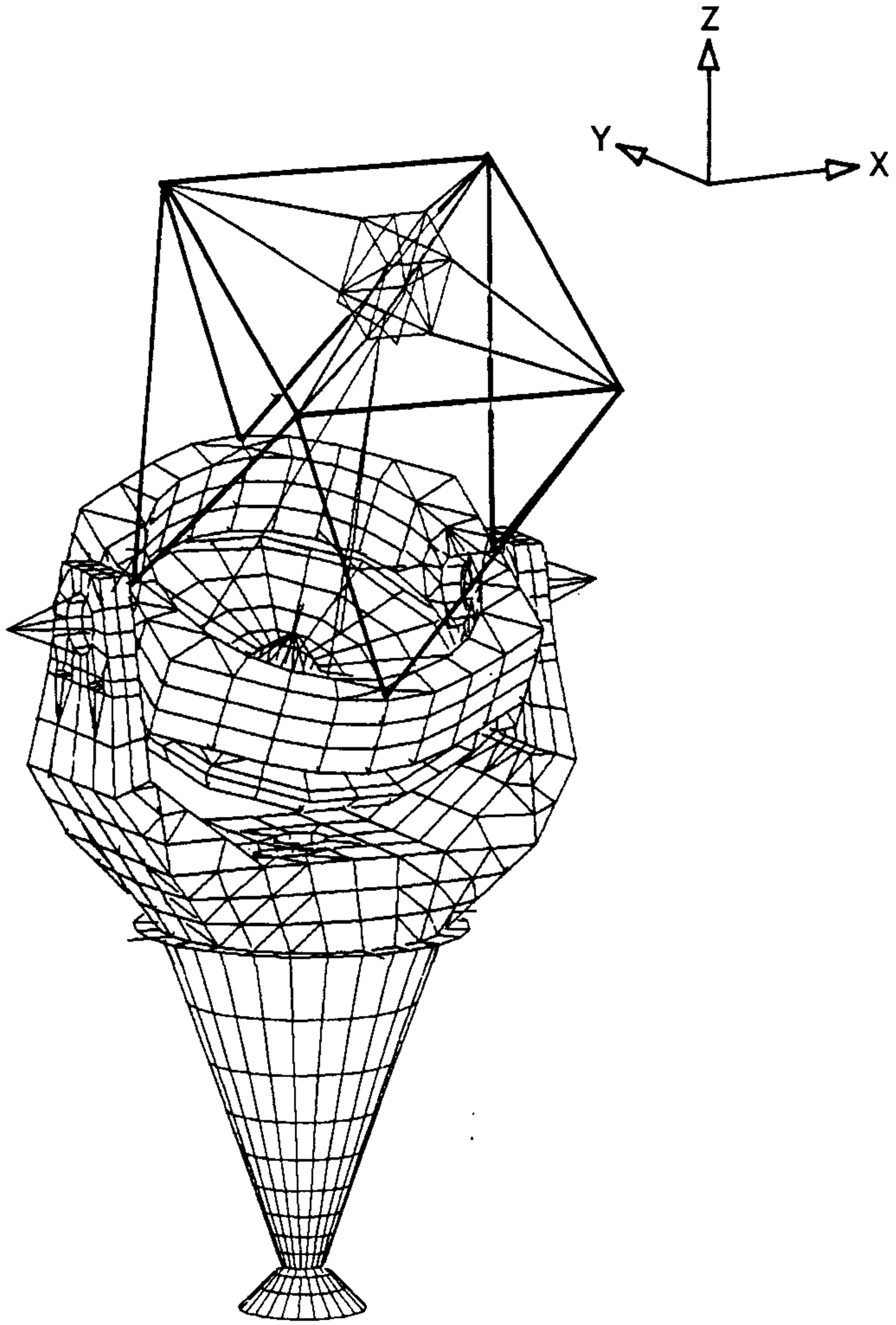


**FIGURE** 1 - Model WIYNTM17, complete telescope model used for modal analysis, shown with hidden lines removed. OSS is 30° from the zenith attitude. Tripod-type primary mirror target and simplified mirror cell were used in modal and wind analyses. Nasmyth instrument masses were applied at the points of the (quadripod) beam elements shown. See subsequent figures for more detailed descriptions of structure.

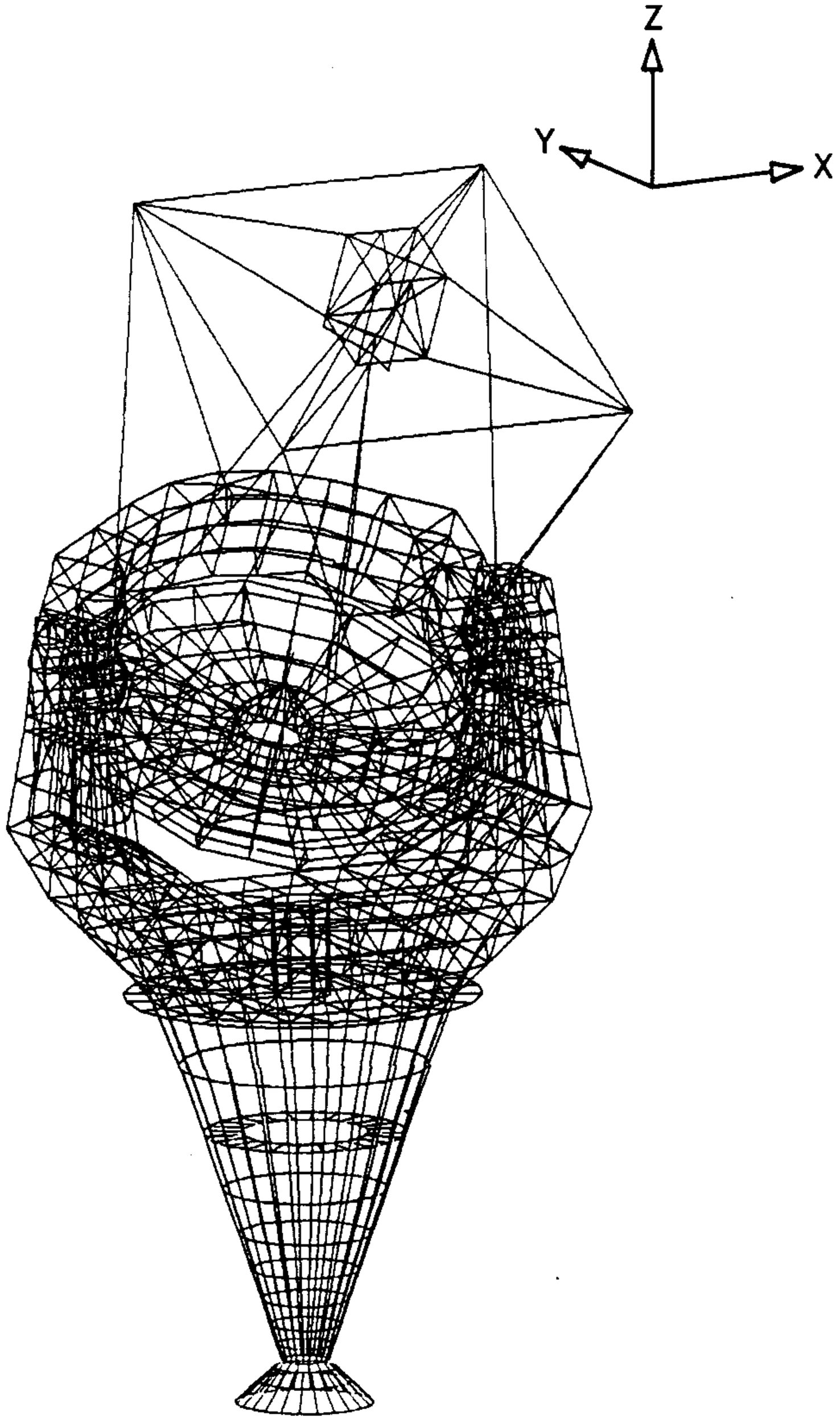


**FIGURE 2** - Model WIYNTM17, without hidden lines removed. Nasmyth instruments and upper azimuth supports are not shown here.

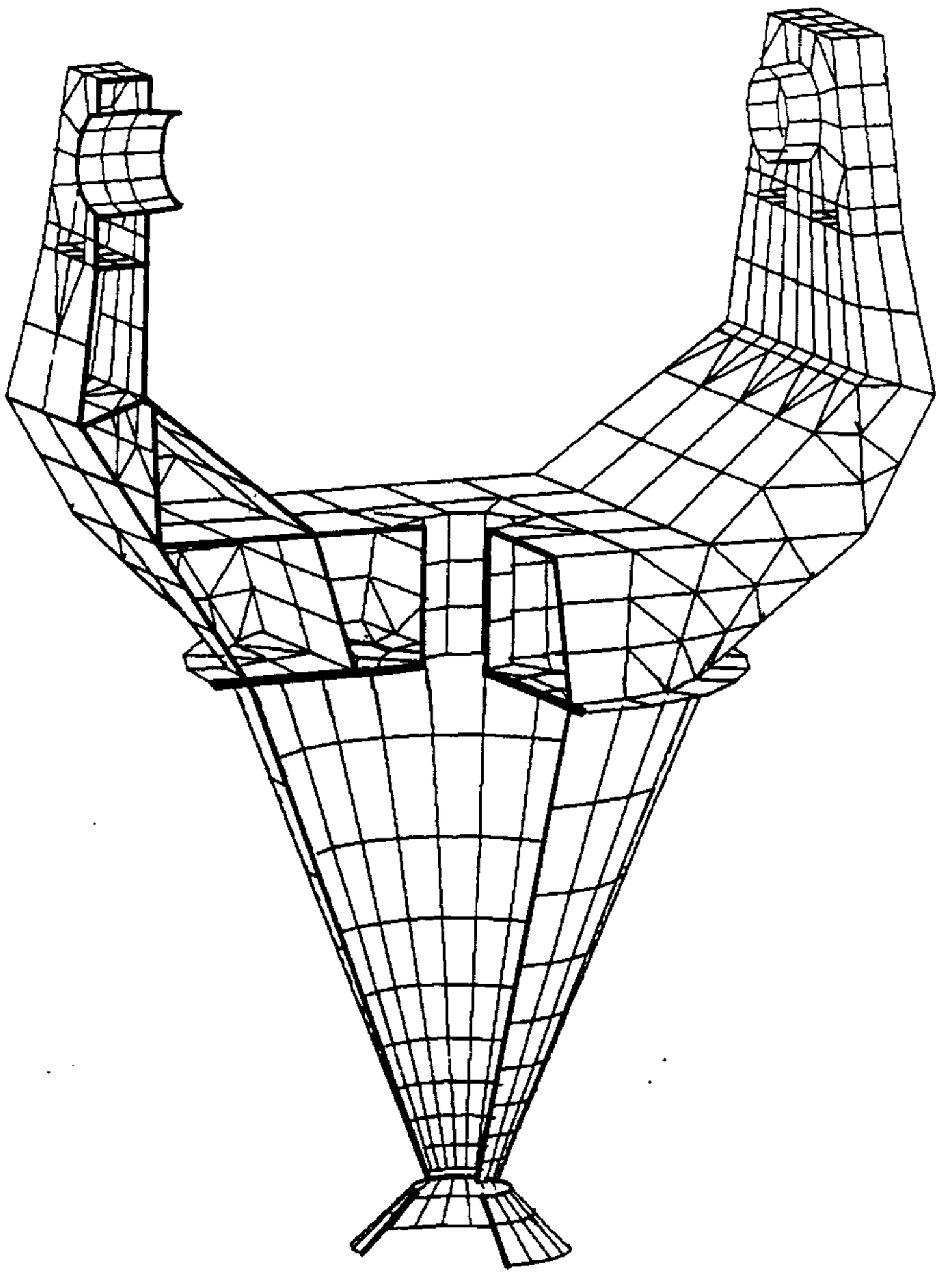

**FIGURE 3 -** Cutaway view of fork. Cone length was increased 20 in. and an internal circular ring added to model during FEA optimizing, not reflected in this earlier graphics plot. Mechanical (bolted) joints are located as described in subsequent graphics plots.

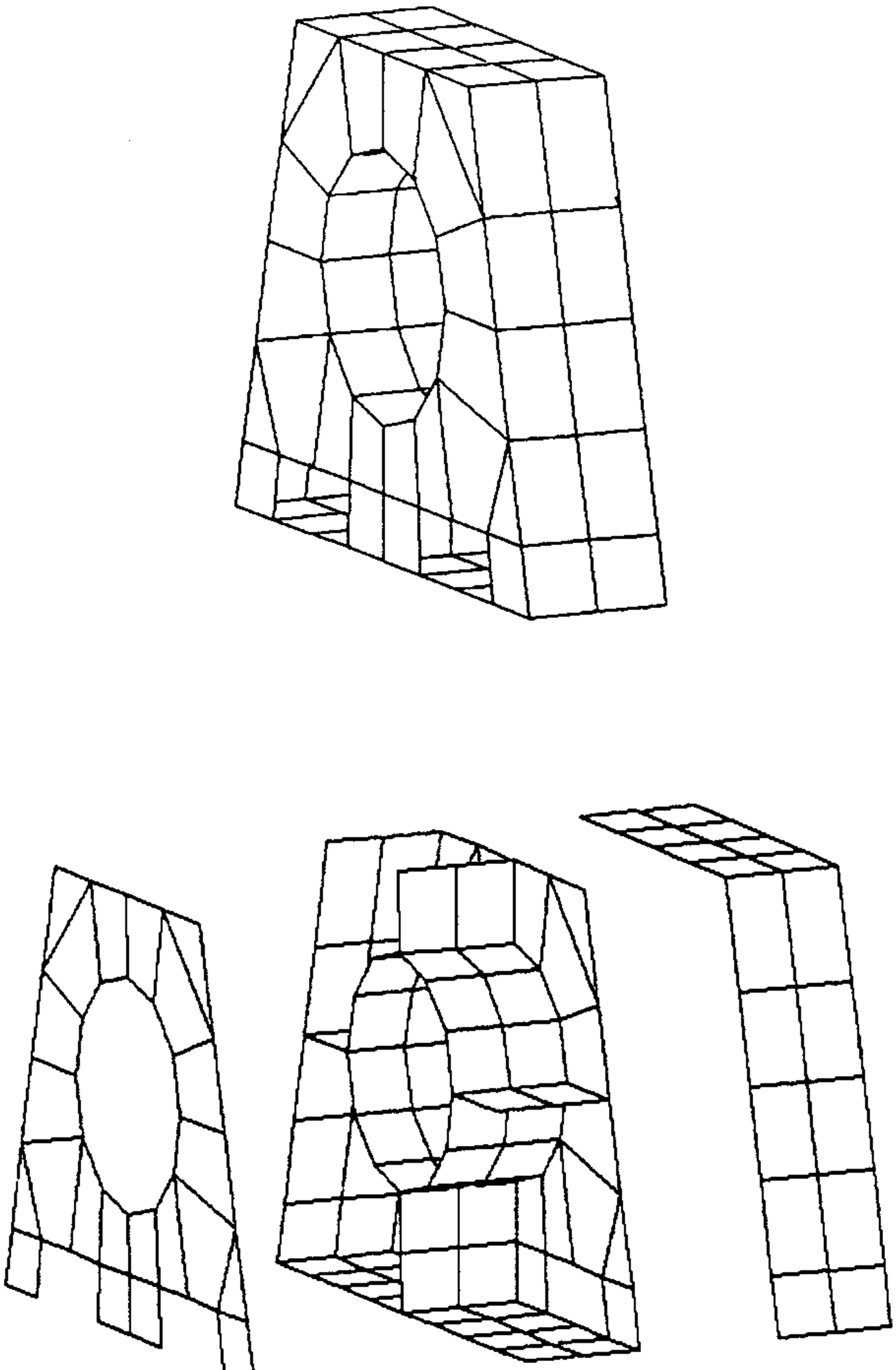

**FIGURE 4** - Exterior and exploded views of one pillow block, which bolts to the top of each fork tine. Bolting access holes are provided near the bottom of the large vertical plates. All plate elements in the model were 1/2" thick except the axle support tube (2.25") and the bottom plate, made 2.75" thick to represent the combined thickness of the pillow block bottom plate and tine top plate.

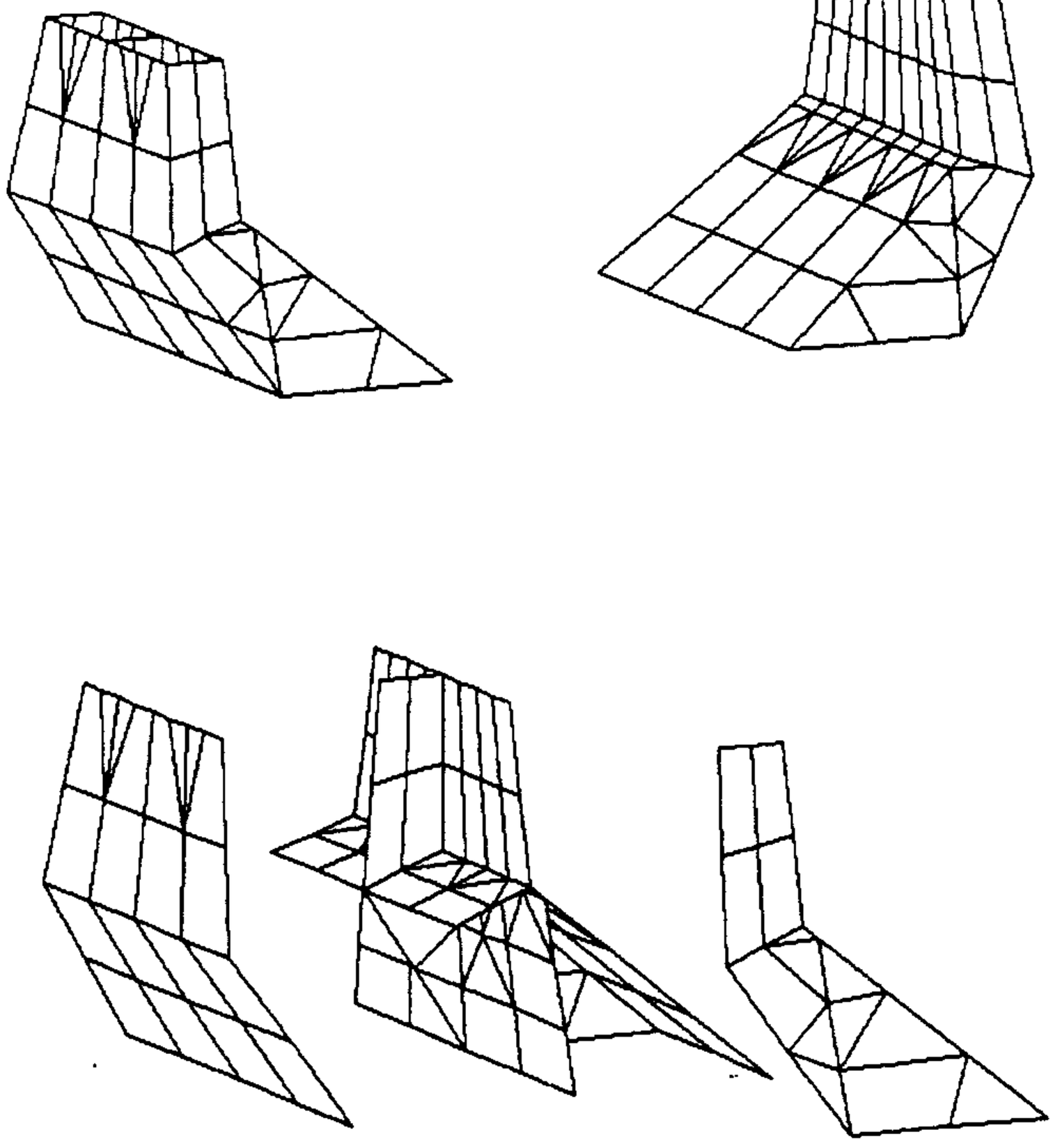

**FIGURE 5** - Exterior and exploded views of the fork tines. These are planned as being integral with the horizontal "throat" of the fork (also referred to as the "base") in a single weldment. All plates were modelled as 1/2" thick except the internal slanted plate tieing the inner and outer plates at the "knee" of the bend, which was modelled as 3/4" thick.

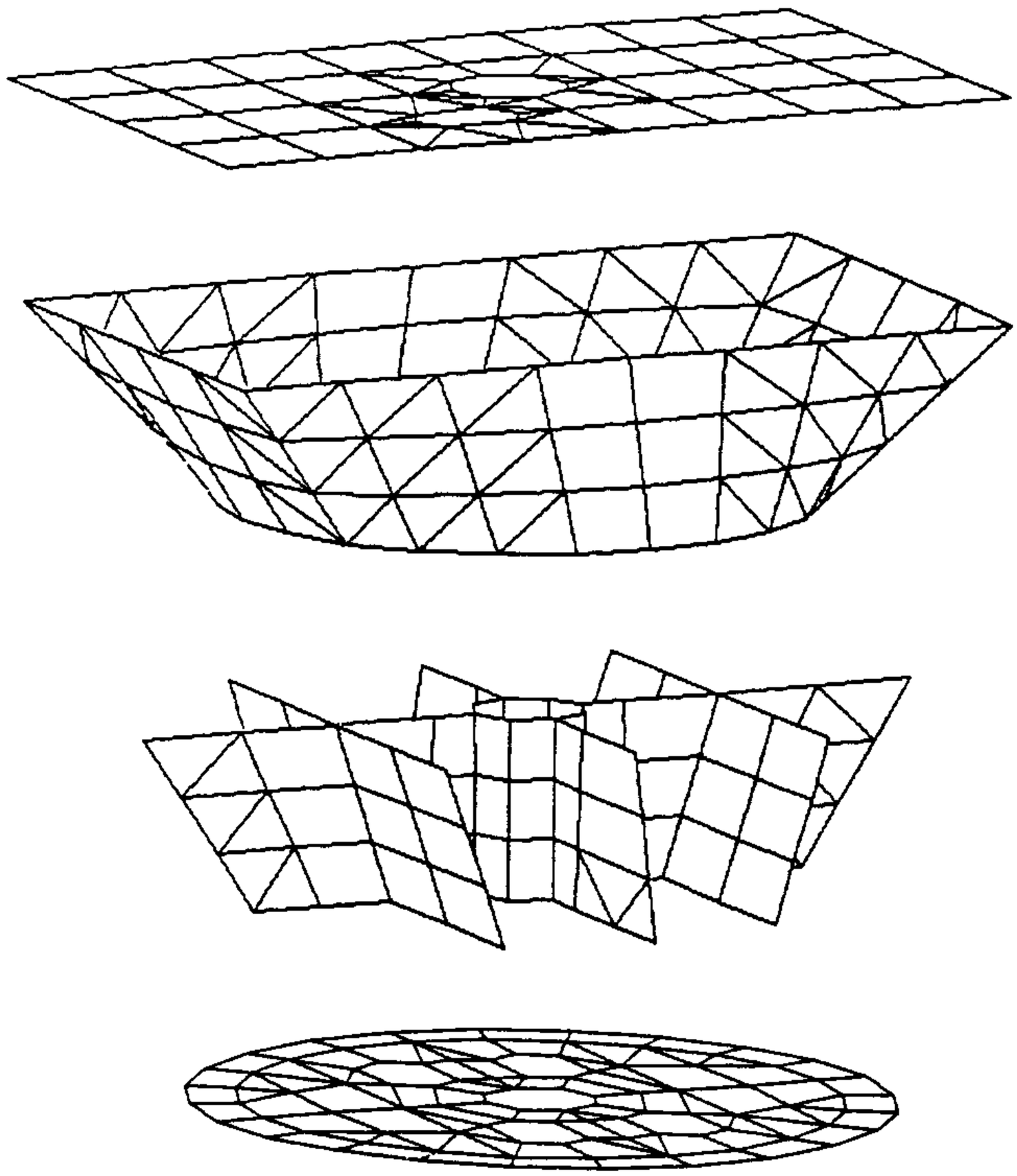

**FIGURE 6** - Exploded view of the "base" portion of the fork. The top horizontal plate is 3/4" thick and includes a 15" x 22" hole for personnel access into the fork and lower cone. The outer shell is a transition which is rectangular at its top end and circular at its lower end, and is 3/4" thick. All internal plates are 1/2" thick except the central tube for utilities clearance, which is 1/4" thick. The bottom plate of the real weldment is planned as 1 3/4" thick except near the edge, where it is machined to 1 1/8" thick. The azimuth drive disk in the real telescope is planned as 1 5/8" thick in the central area and 2 1/2" thick at the rim. These two plates were combined in the model as a single 2" thick plate with a steel modulus, but artificially high mass density. Note that the center of the bottom plate ties to the internal webs and the central tube, and that there are four 15" x 22" oval holes to allow personnel access to the base (from the cone) for routing utilities, etc.

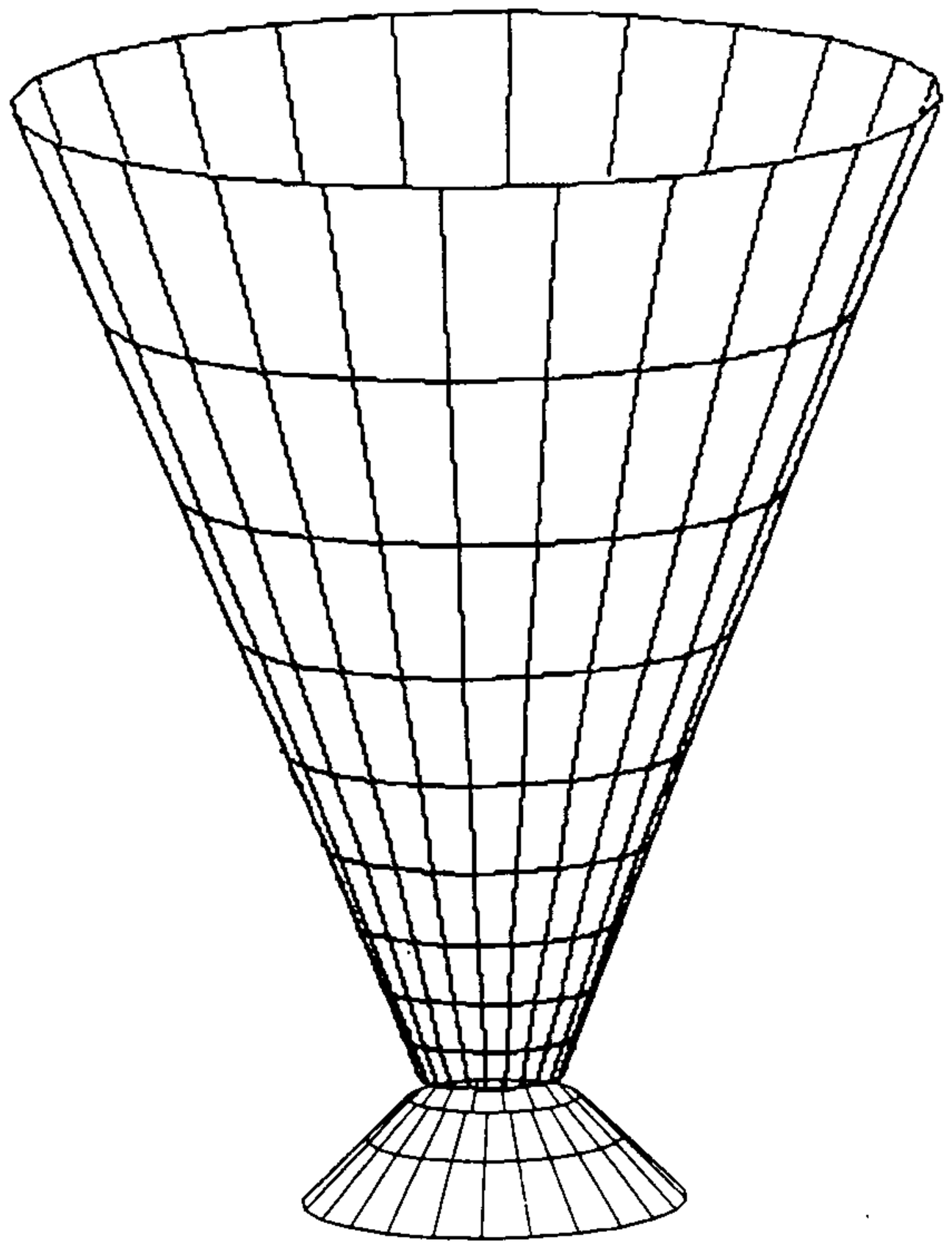

**FIGURE 7** - Cone and lower bearing support pedestal. All elements are 3/4" thick except that the pedestal and lower area of the cone are 1" thick. An internal circular ring was added in the cone to minimize its distortion for certain modeshapes, and which would be required in the real telescope as a manufacturing aid.

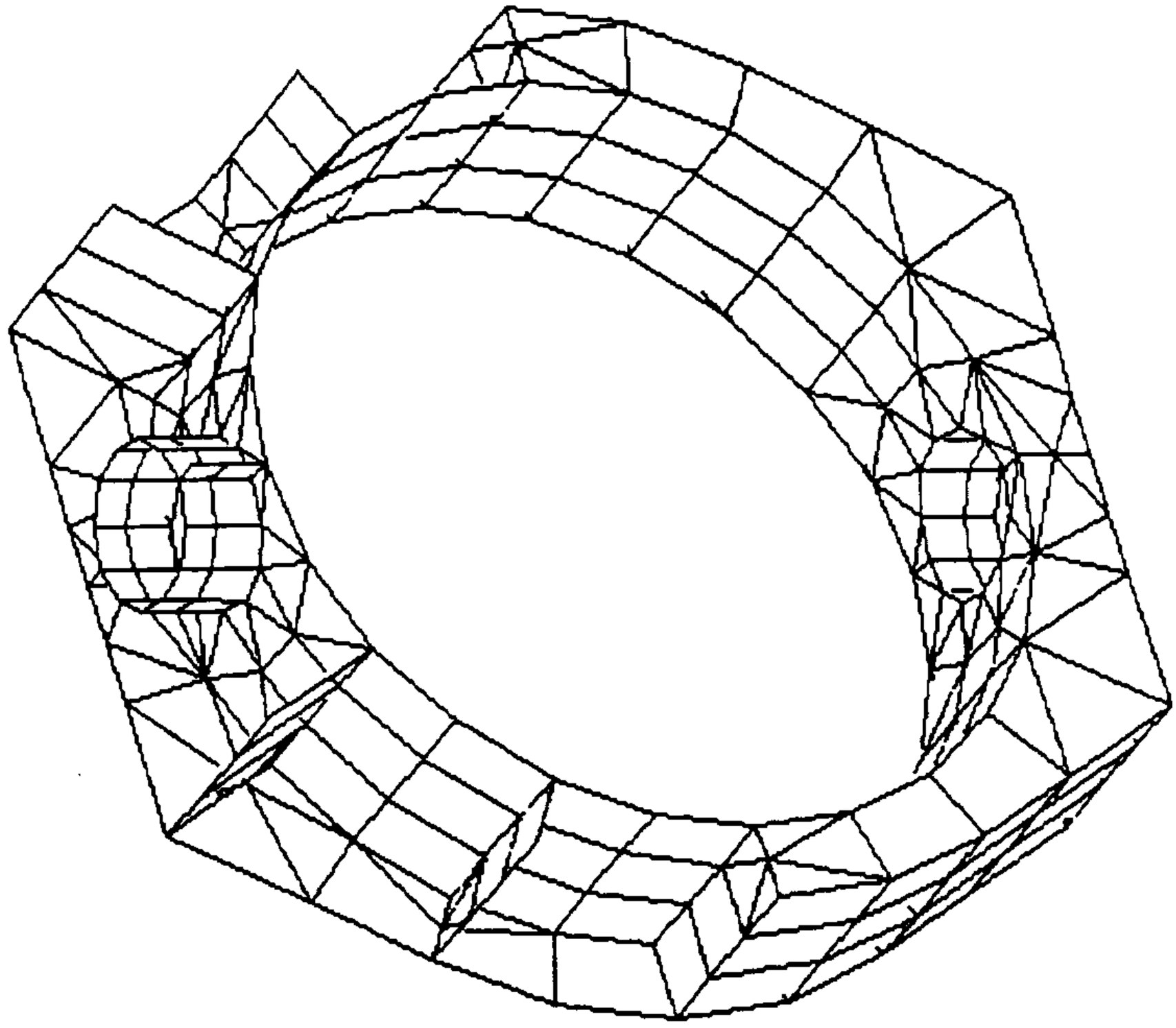

**FIGURE 8** - Center section of the Optics Support Structure, with external plates removed in the near half. All plates are 3/8" thick except that all internal gussets are 1/2" and the bearing support tube has varying thickness as shown on drawing E305007 sheet 2. Note that the third instrument position to be mounted on the top side of the center section was not modelled, on the assumption that its effect is negligible. Such an effect would likely be included in the final (detail design) finite element model.

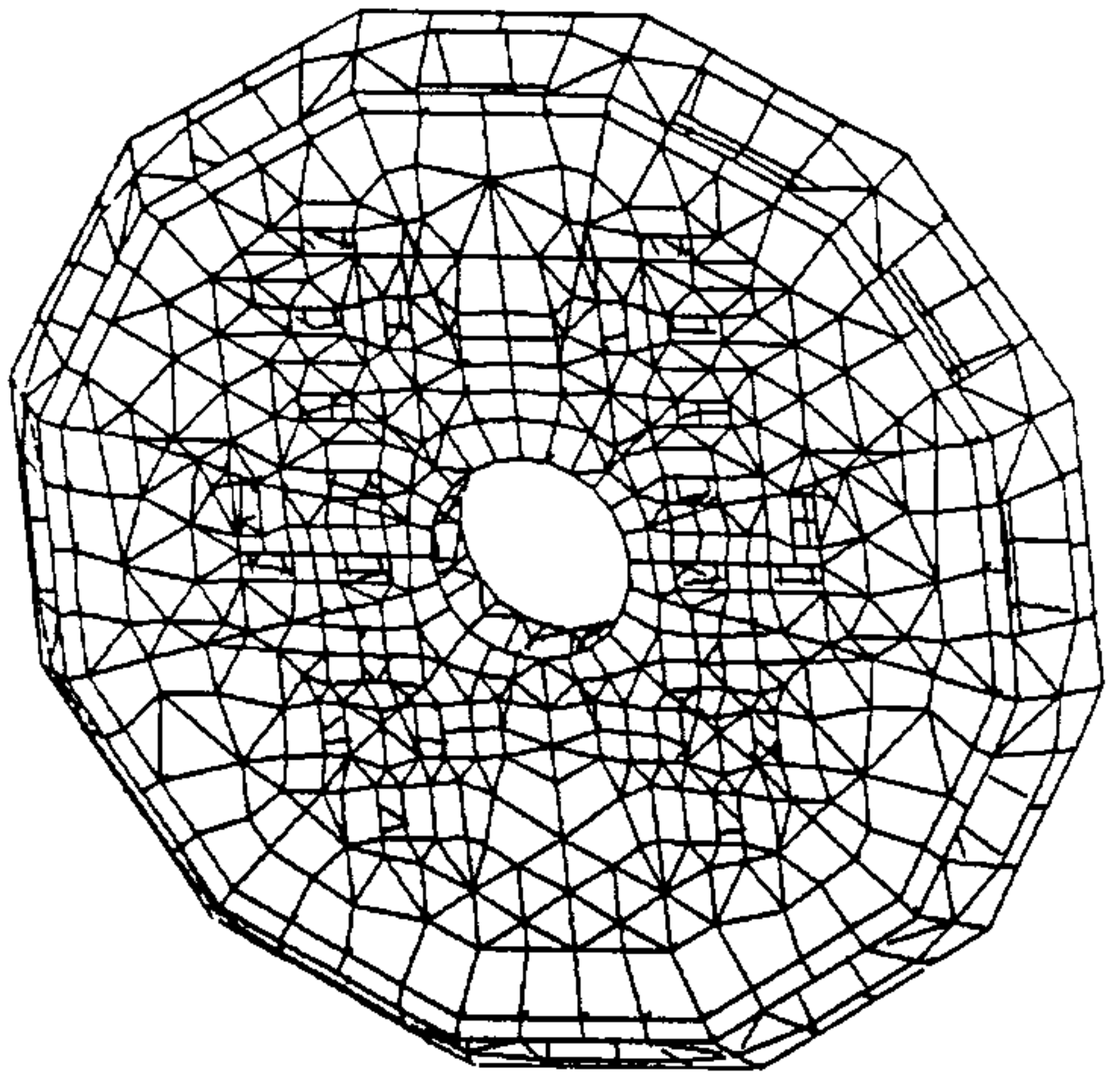

MIRROR CELL - BACK VIEW

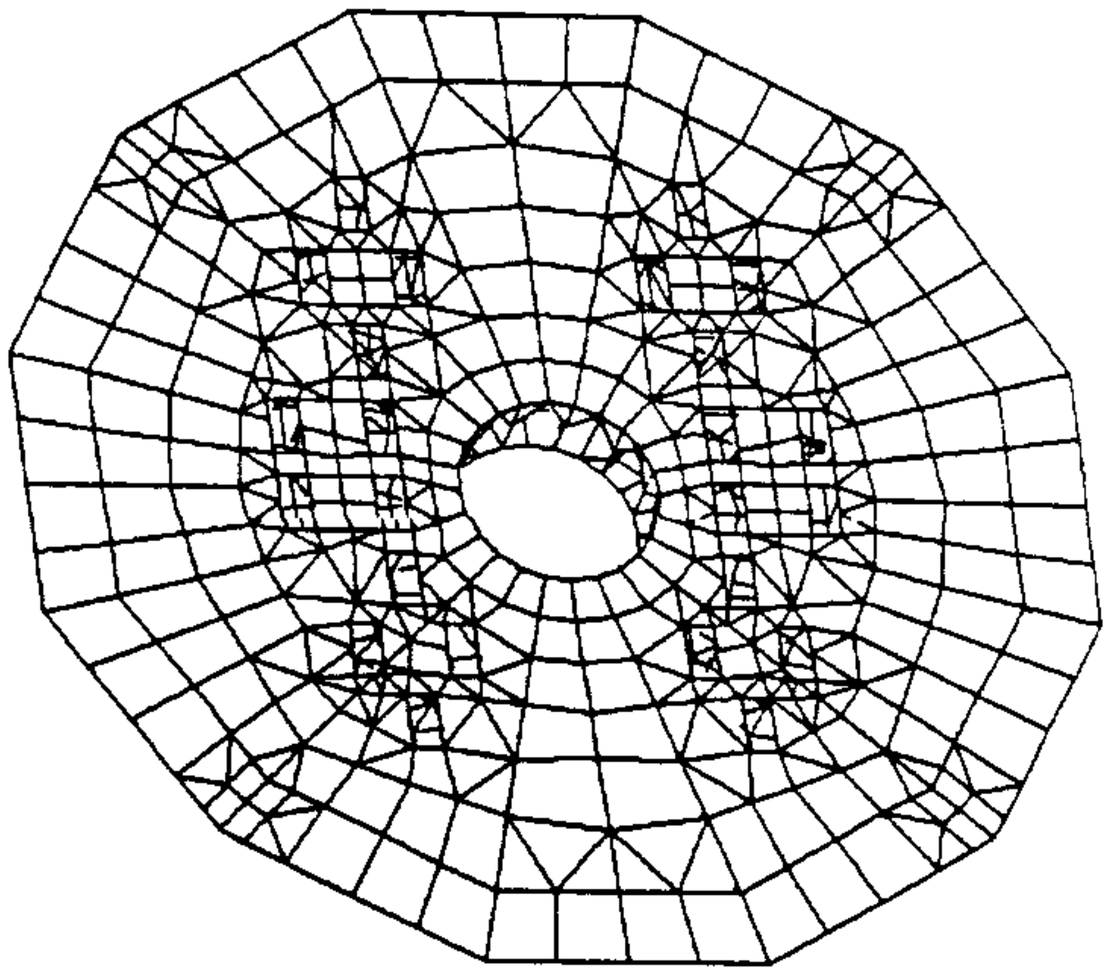

MIRROR CELL - FRONT VIEW

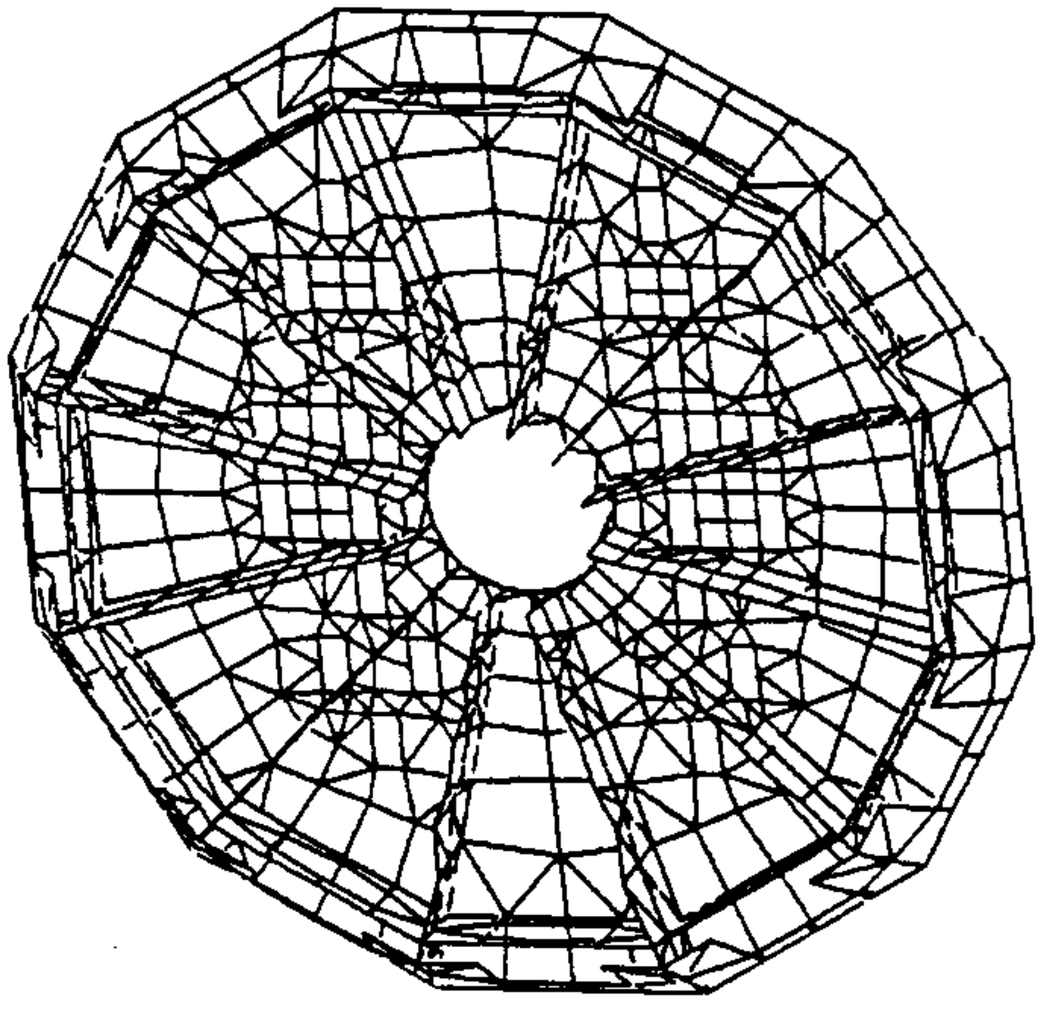

BACK VIEW, BACK PLATE REMOVED

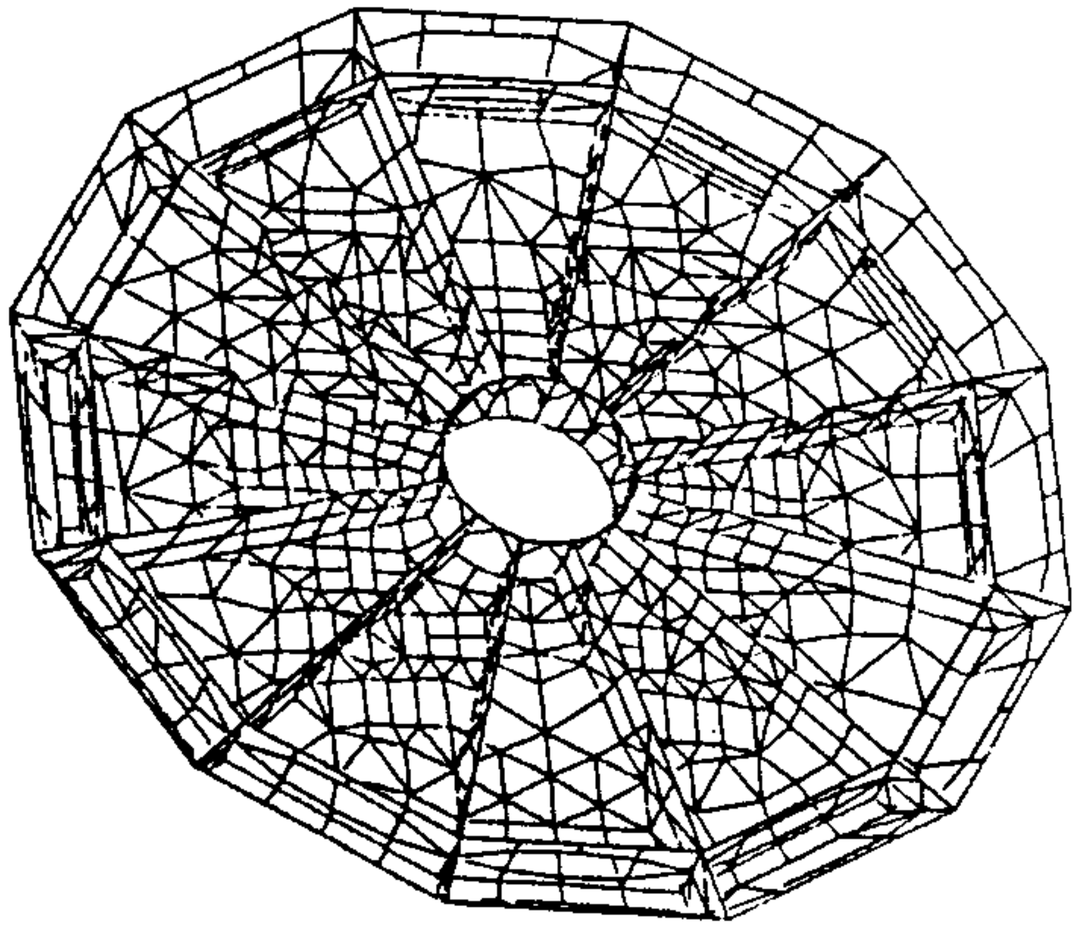

FRONT VIEW, FRONT PLATE REMOVED

**FIGURE 9** - Mirror cell model used in model WINOSS1, the gravity loading finite element model. Complex mesh was required to interface with model of primary mirror support system (described in body of text). Plate thicknesses are as defined on KPNO Dwg. 3500.0002073E. Tube lining center hole was subsequently made solid, not reflected in this earlier graphics plot.

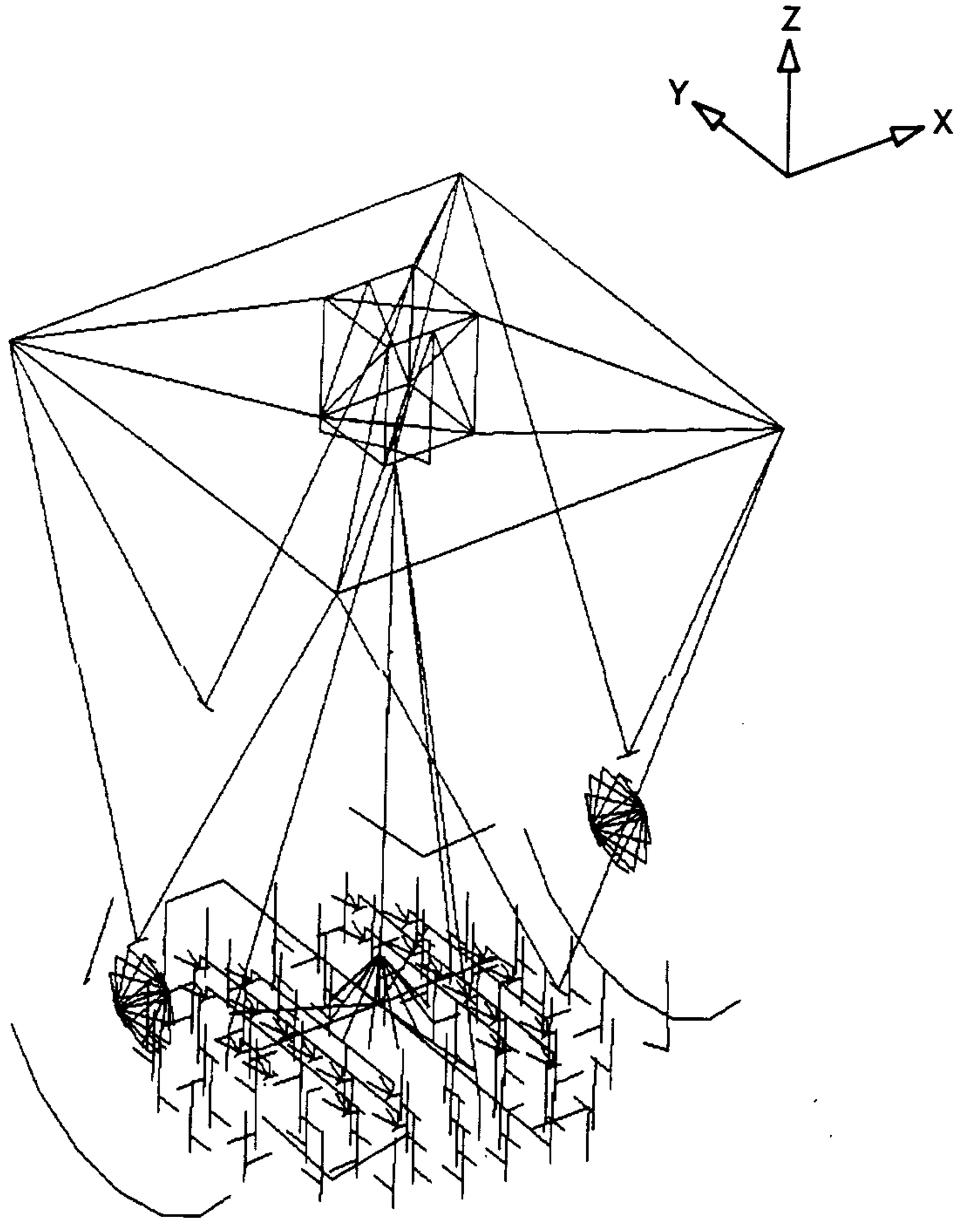


**FIGURE 10 -** All 648 beam elements in model WINOSS1, the gravity loading model of the Optics Support Structure. Many elements are used to define spring rates such as in the mirror support system and altitude bearings. Detailed descriptions are included in the following graphics plots.

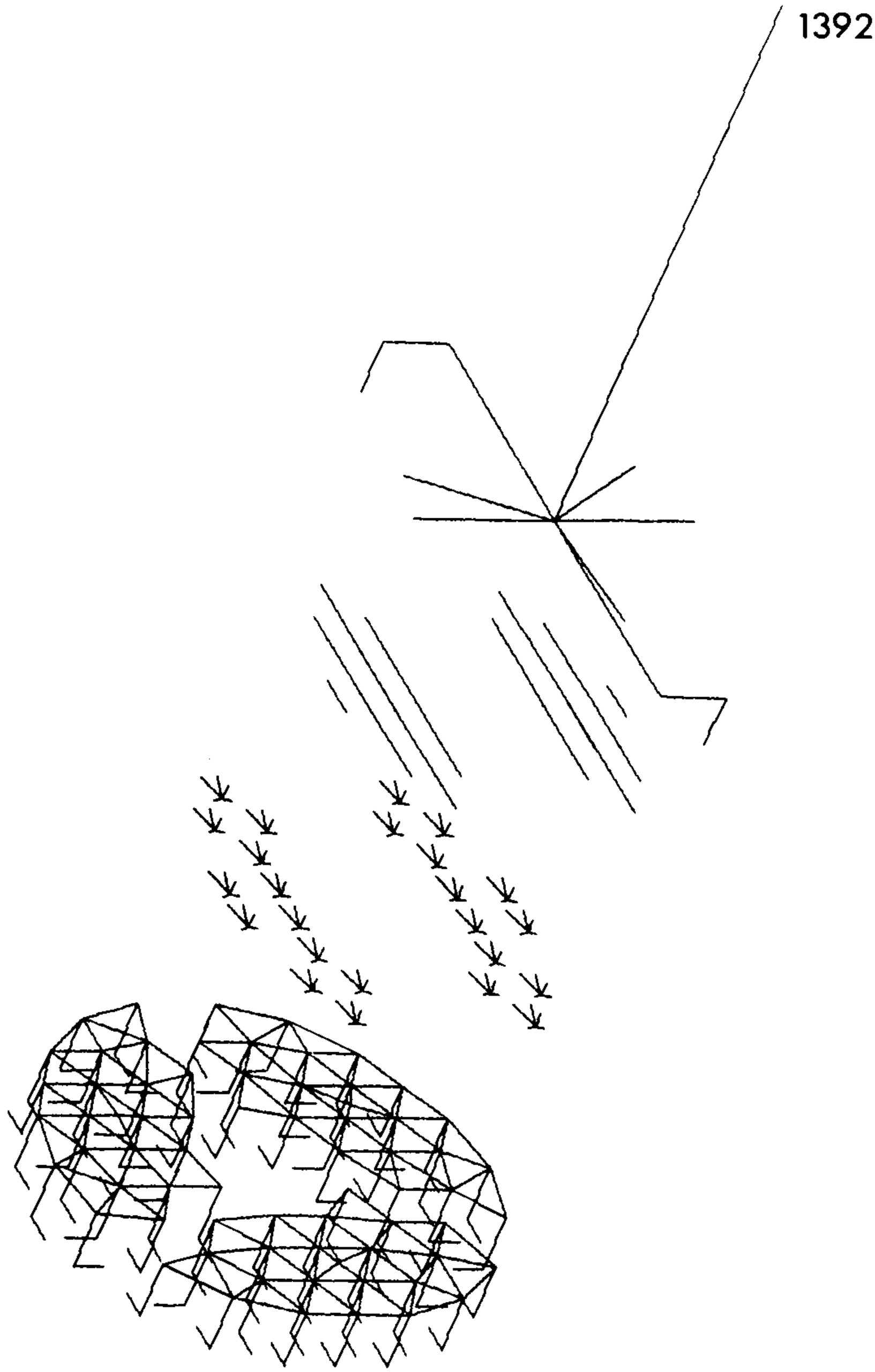


FIGURE 11 - An exploded view of the 381 beam elements used to define the mirror support system and primary mirror in model WINOSS1. The lower group includes axial support system beam and sector plate elements, and axial support unit stiffeners. The next group are lateral support brackets and supports. The third group is used to simulate the hydraulic sharing of the lateral system. The final group is the rigid primary mirror including the collimation links. Node 1392 is the primary mirror target at the secondary mirror vertex. A detailed description is provided in the body of the report.

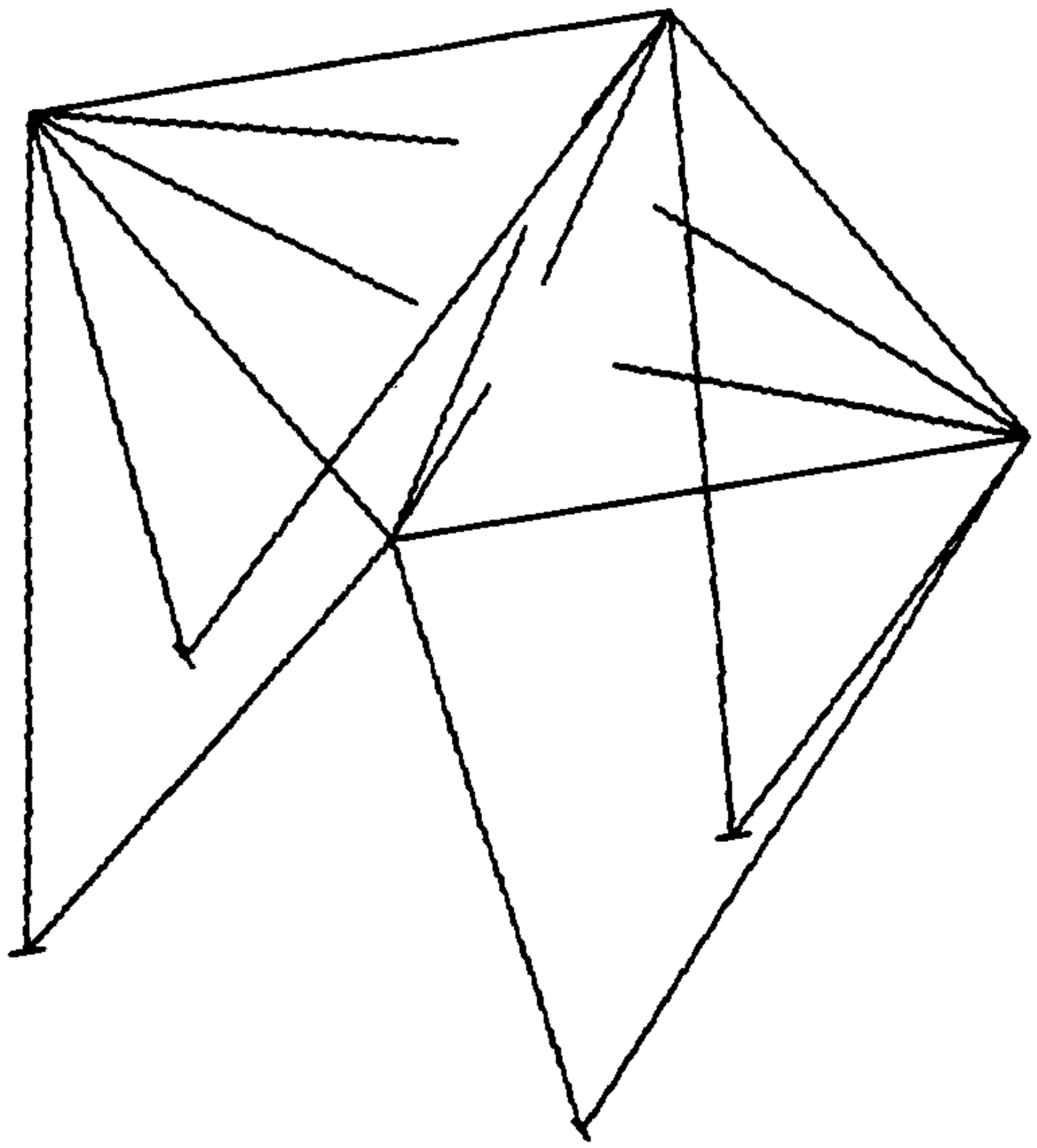

**FIGURE 12** - The secondary end beam elements less the center structure. The main truss and square frame use 4" outside diameter x 1/2" wall tubing. The lower vanes are 1/2" x 3" flat bar, the upper vanes 1/2" x 1 3/4" flat bar.

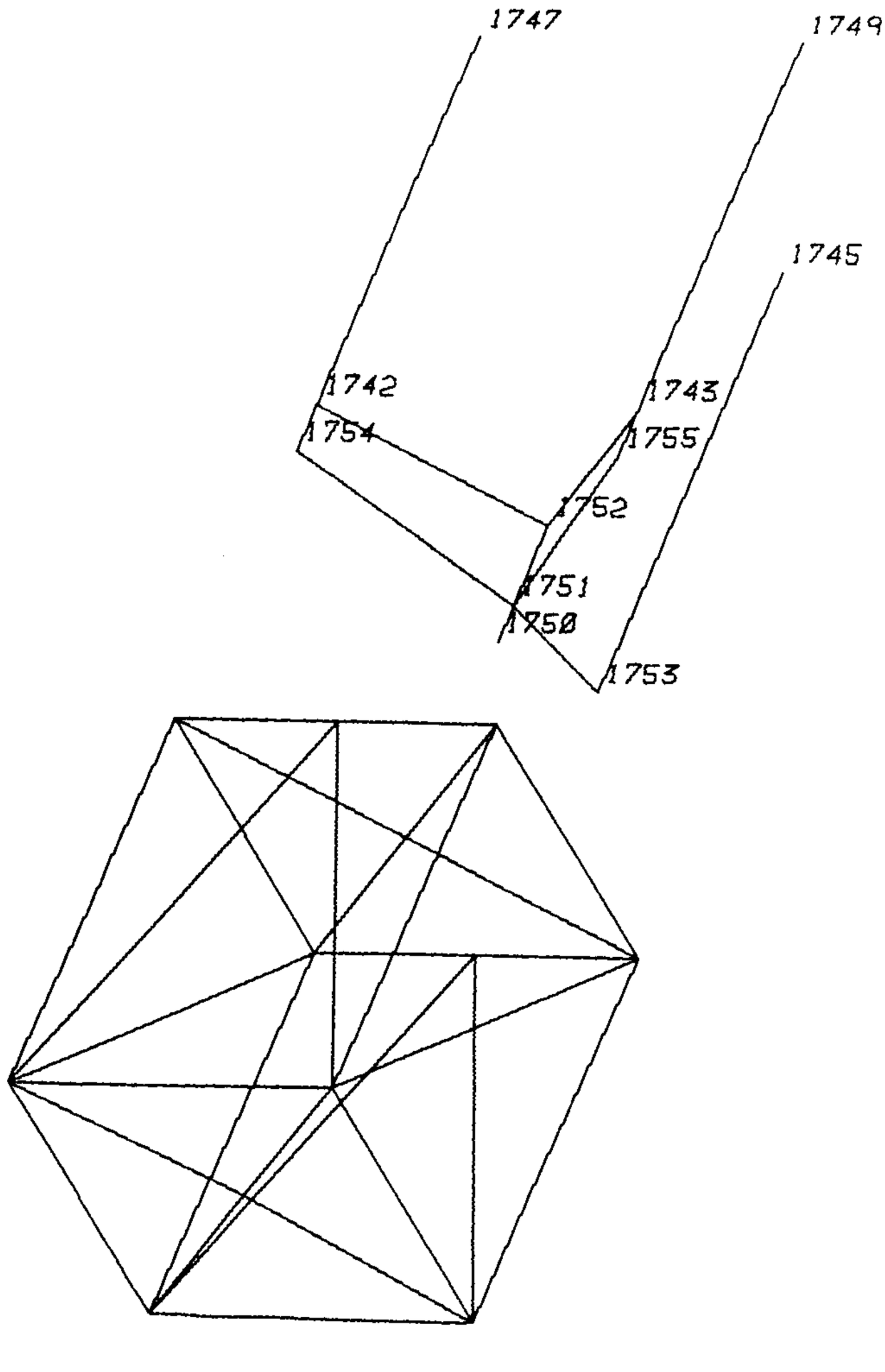


**FIGURE 13** - The secondary center structure with the secondary mirror and supports removed and shown above. All members in the center structure are structural tubing, TS 2 x 2 x 1/4" except for the "x-braces" on the ends, which are 1/2" x 1 3/4" flat bar. The secondary mirror (and cell) were modelled as rigid. The axial supports (including actuator, pushrod, and flexures, such as from node 1747 to 1754) have a net spring rate of 115,000 lbs./in. The lateral supports are collimating links (such as node 1742 to 1752) at 217,000 lbs./in. Node 1750 is the secondary mirror target (secondary vertex).

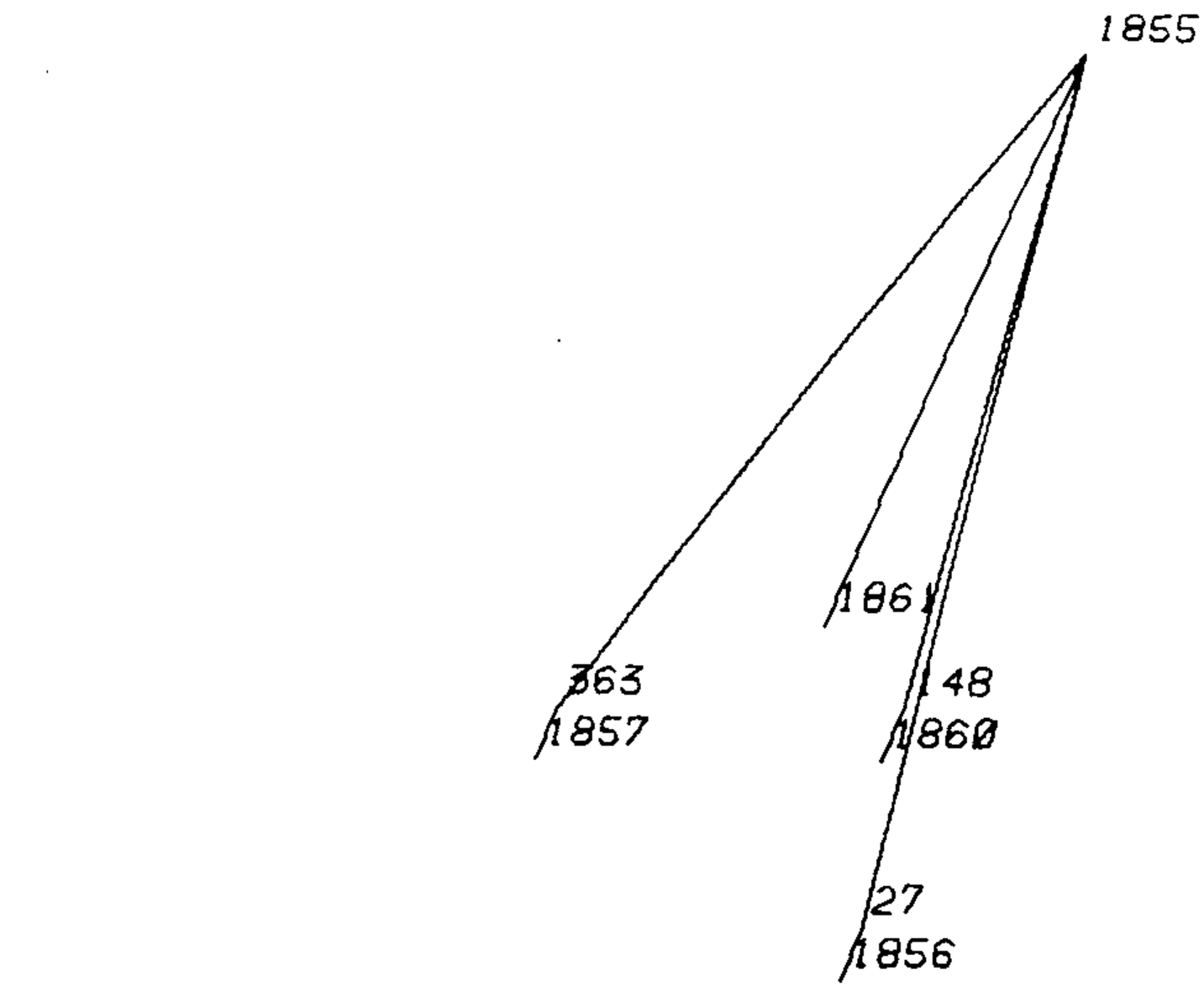


**FIGURE 14** - The alternate "primary mirror target" to determine optical alignments if support system effects are eliminated. This tripod attaches directly to cell at three reference points. Structural tubes in cell connecting the front and back plates at these three locations are also shown. Node 1855 is the alternate primary mirror target.

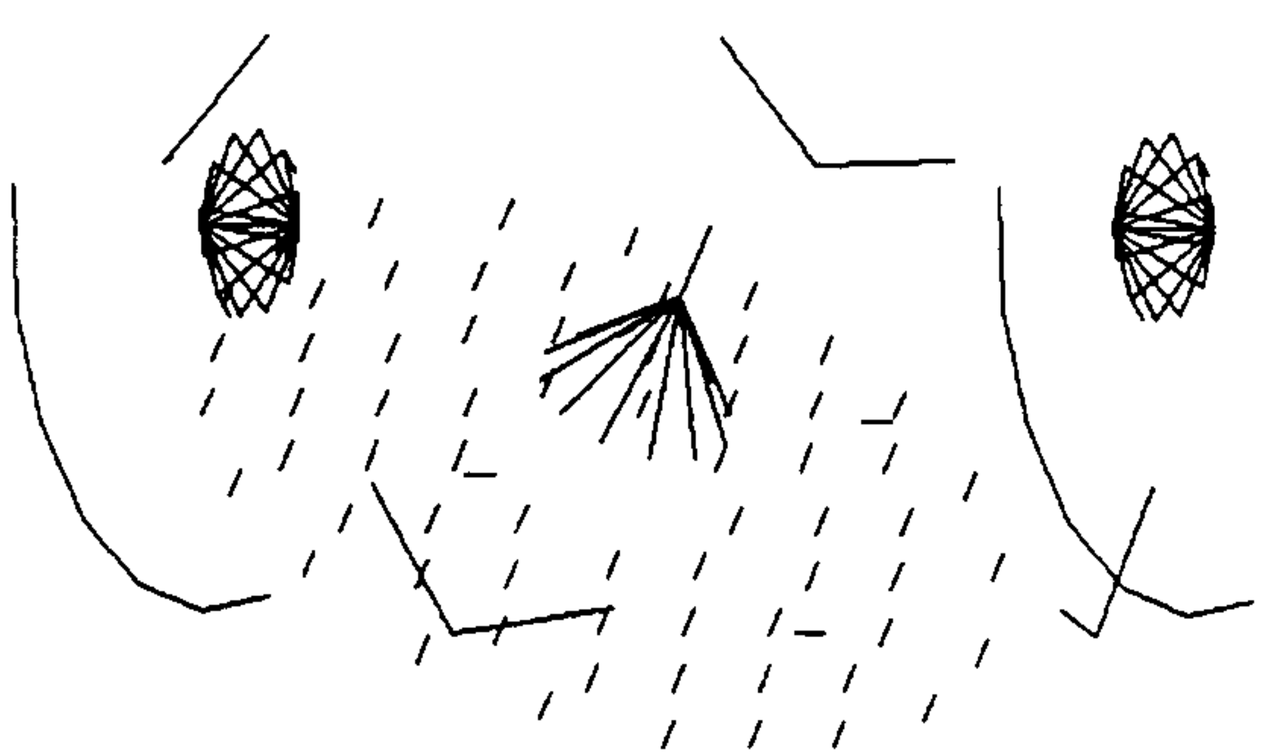

**FIGURE 15** - Remaining beam elements in model WINOSS1, including axial support c.g. supports, tertiary c.g. support and target, altitude bearings, main truss members (4" outside diameter by 1/2" wall tubing), sector antirotation elements, and altitude drive disk rim elements.

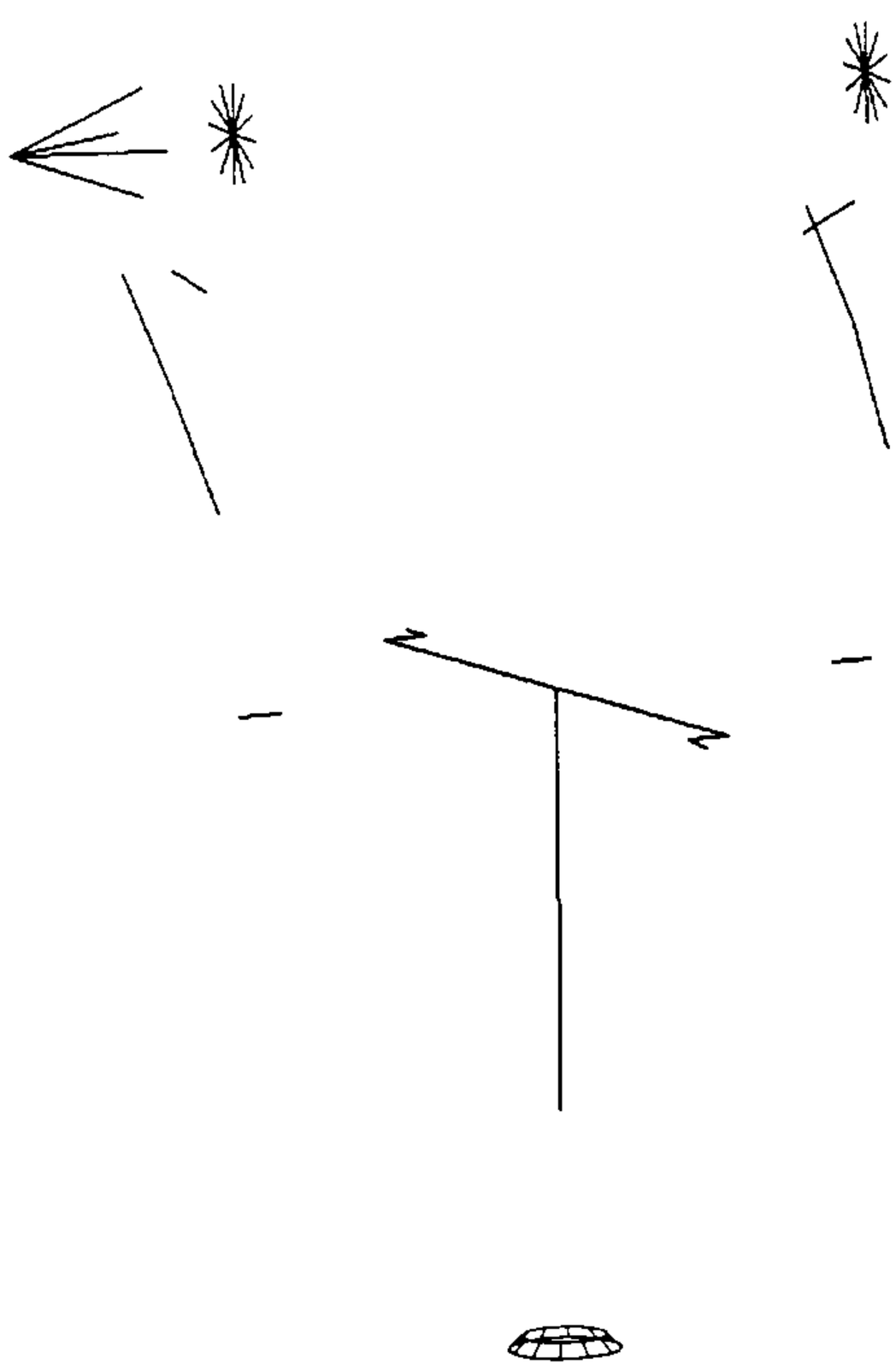

**FIGURE 16** - All beam elements associated with the fork structure in model WIYNTM17, used for modal analysis. Elements are (starting at the top of the view and working inward and downward): Nasmyth instruments, altitude bearing adapters, altitude drive disk support brackets, altitude drives, altitude drive support beams, upper azimuth radial supports, azimuth drive torsional system, and azimuth lower bearing and support rings. Altitude and azimuth drive "locked rotor" stiffness used was 400,000 lbs./in. tangential stiffness for each drive. Upper azimuth radial stiffness used was 1.13E6 lbs./in. for each drive and idler unit. The lower azimuth bearing stiffness used was 5.57E7 lbs./in. (thrust stiffness component), based upon an SKF No. 29292 spherical roller thrust bearing.

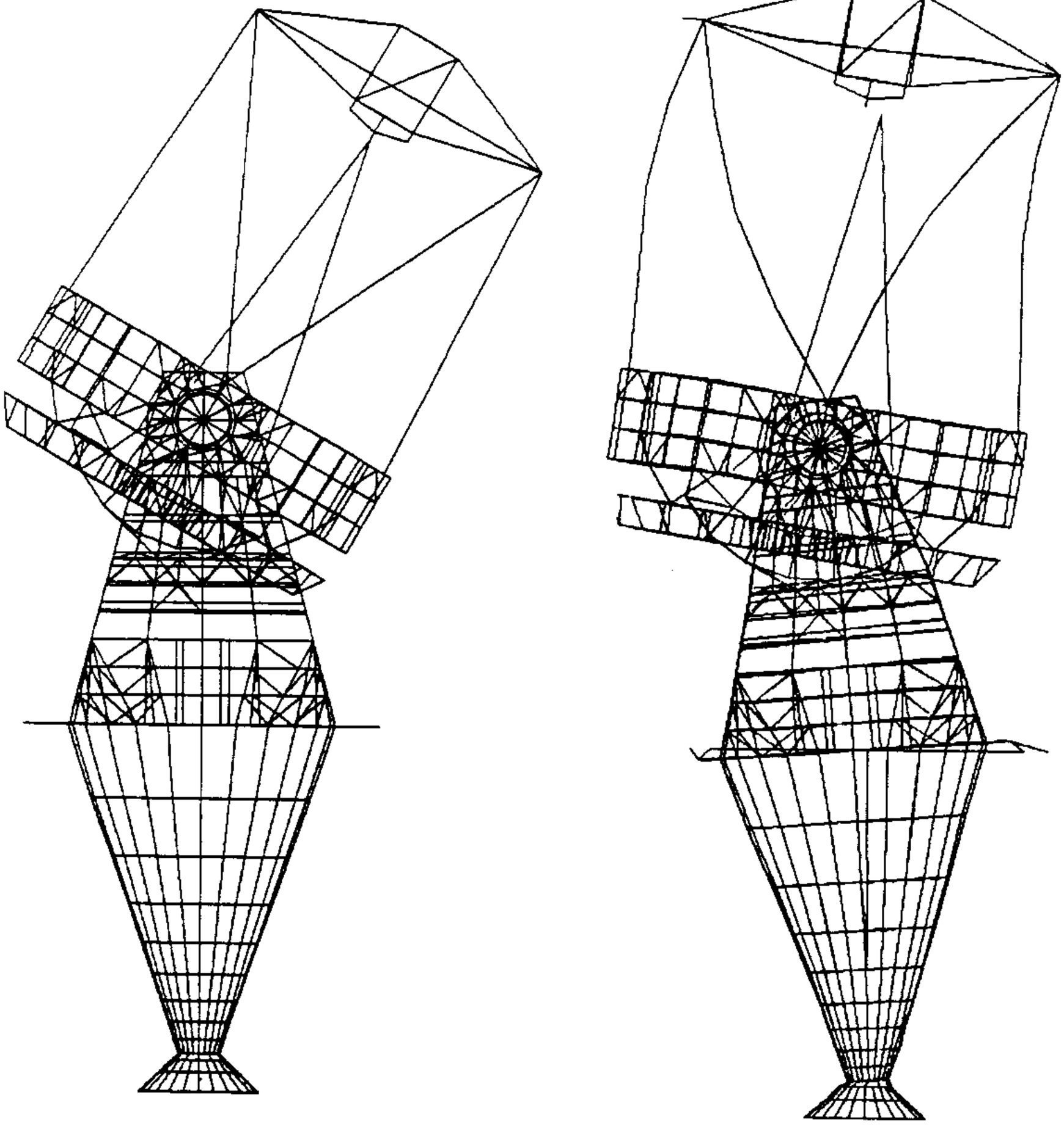

**FIGURE 17** - Side view of model WIYNTM17, the telescope modal analysis model. The left view is of the undisturbed model with the OSS at 30° from zenith. The right view is of modeshape 1, fore-aft translation, at 7.3 hz. Note that the rotation of the OSS (about an axis parallel to the altitude axis) is in phase with the fork rotation, as compared to modeshape 4 (Figure 20), where they are out of phase.

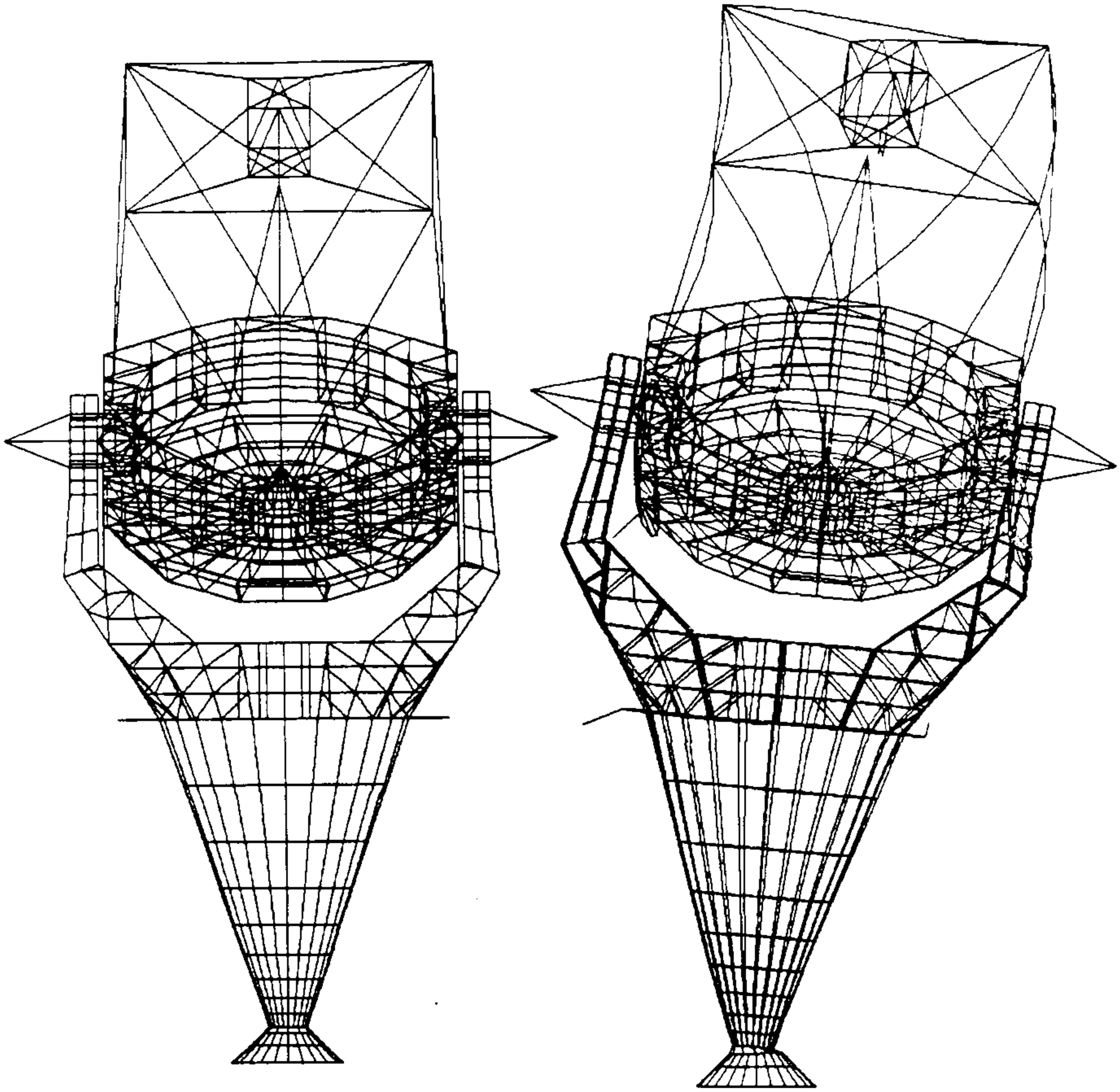

**FIGURE 18** - Front view of the undisturbed telescope and modeshape 2, lateral translation, at 7.6 hz. Some optimizing was performed to increase the primary mode frequencies, although some additional gain can be anticipated in the detail design phase. Note that, while this mode does not couple to either locked rotor mode, there is a noticeable primary pointing error and secondary decenter.

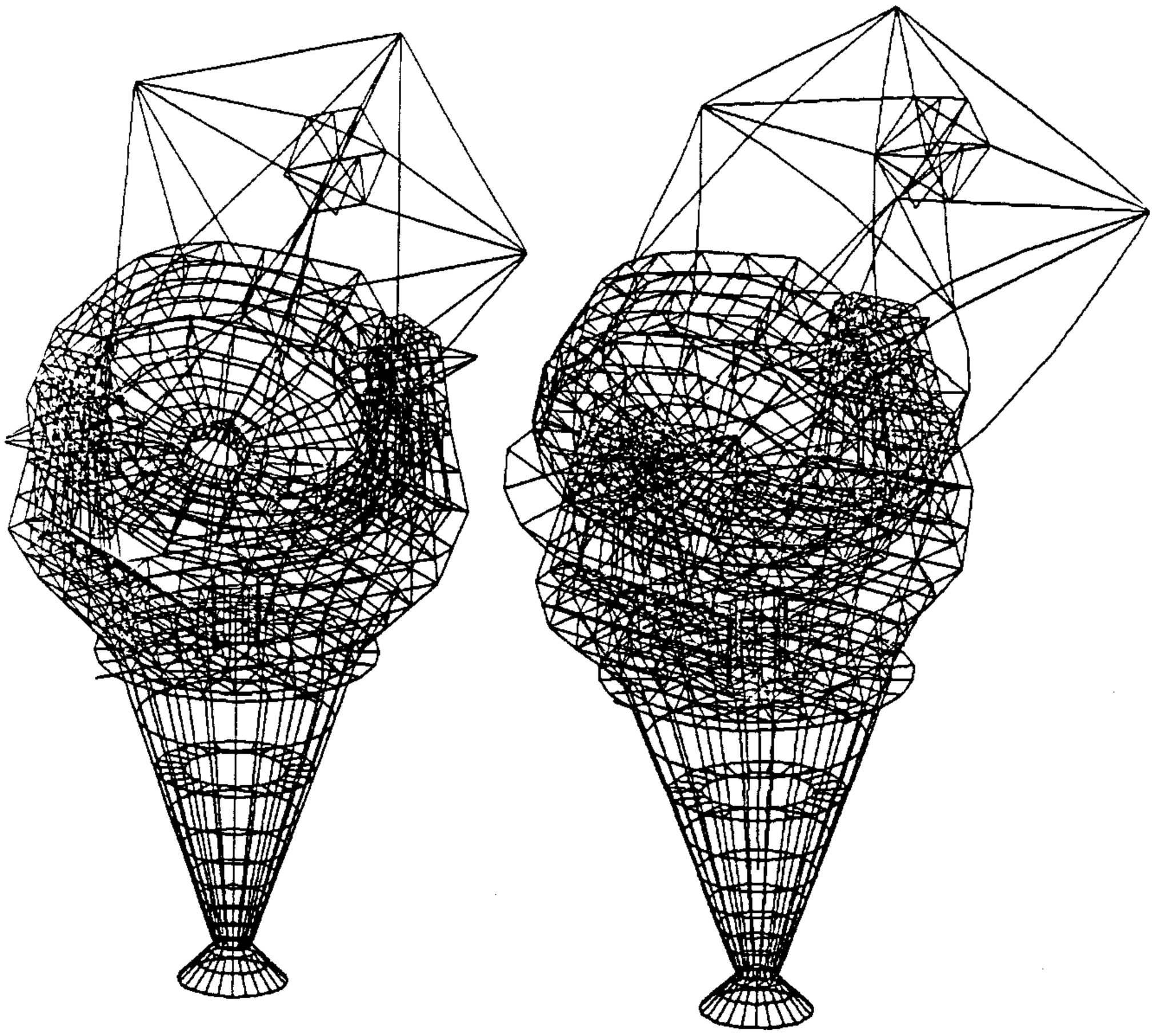

**FIGURE 19** - Quartering view of the system undisturbed (left view) and of the third (primary mode) modeshape, locked rotor rotation about the azimuth axis, at 8.8 hz.

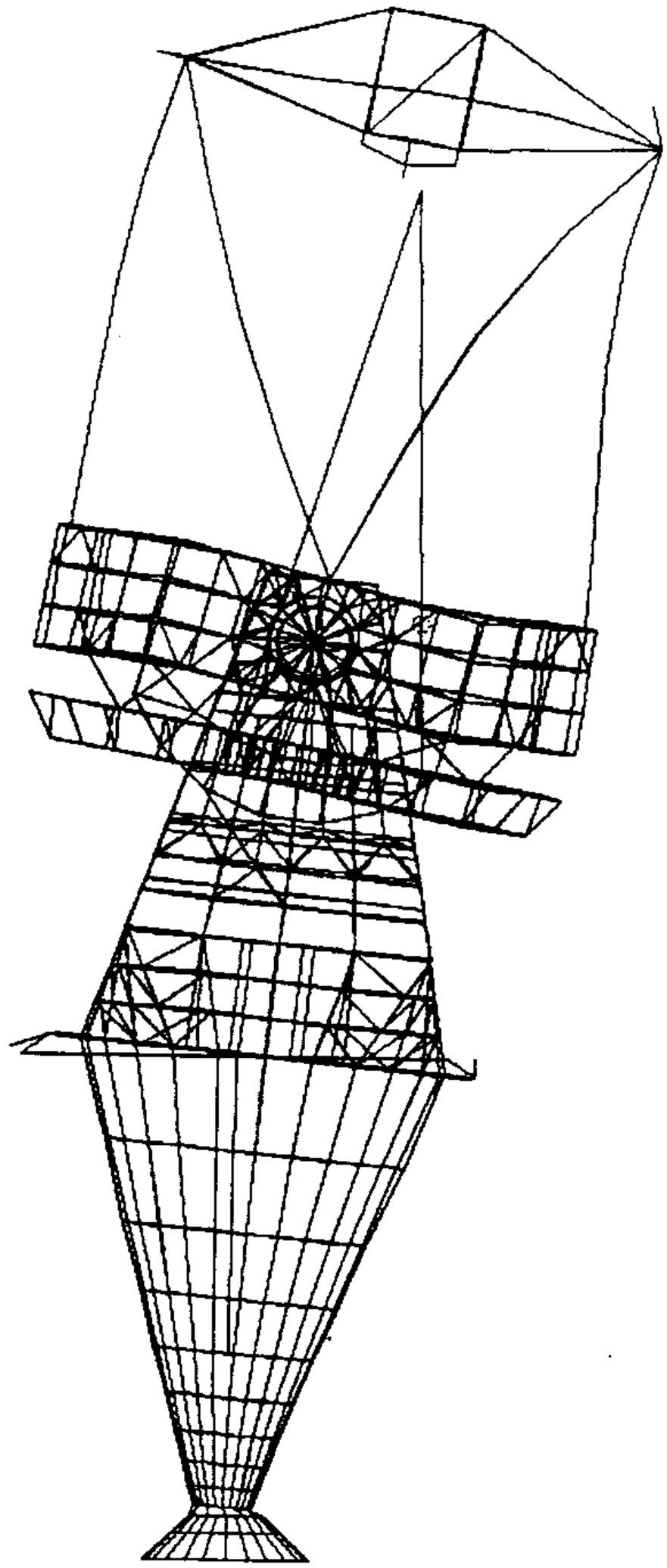

**FIGURE 20 -** Mode no. 4, locked rotor rotation about the altitude axis, at 10.6 hz. Note that the OSS rotation is out of phase with the fork rotation, as compared to Figure 17 ("fore-aft translation").

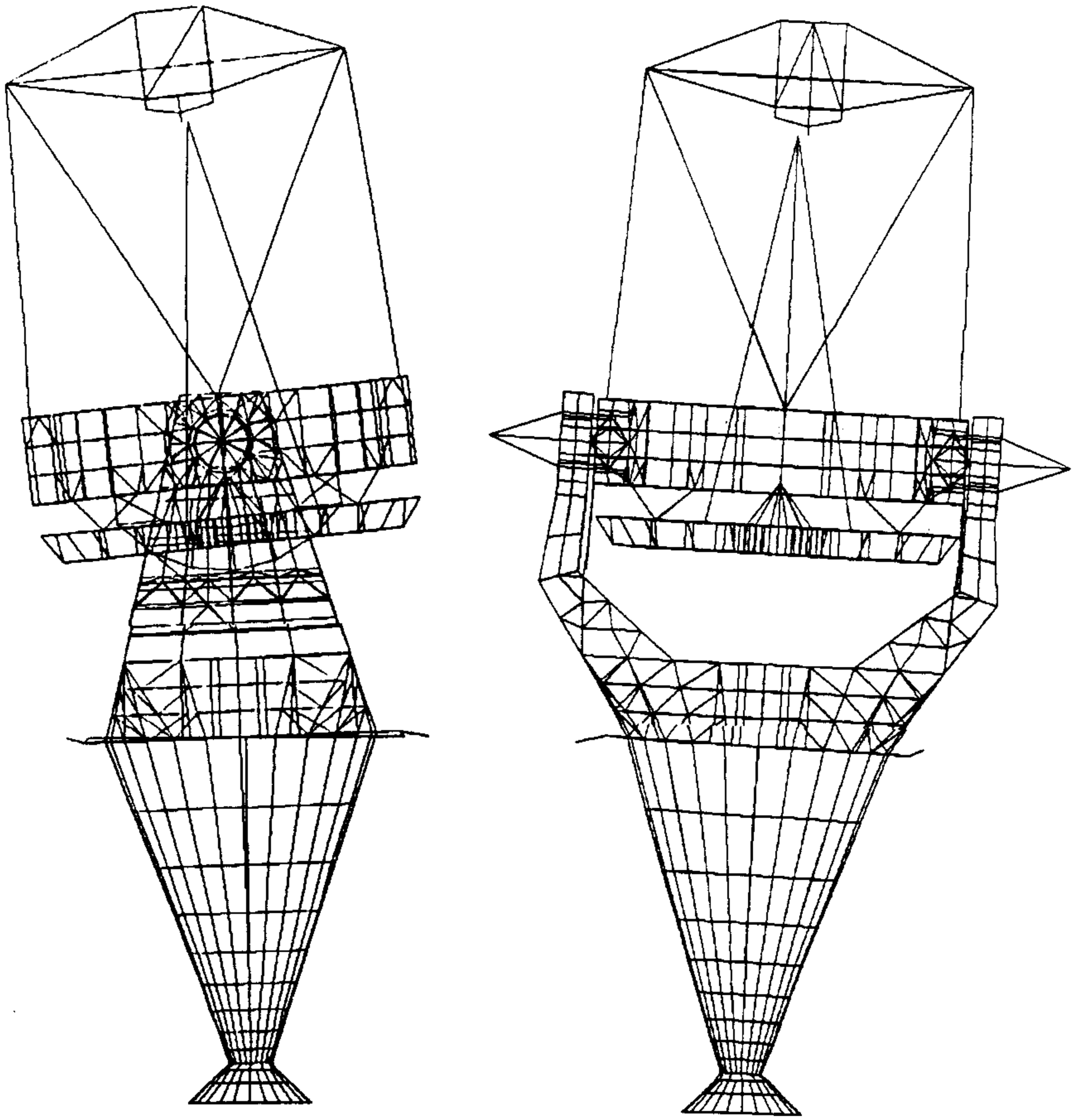

**FIGURE 21** - Model WIYNTZ - the complete telescope, zenith pointing, under wind load. Applied wind load was 15 mph *acting upon the telescope structure*. This is equivalent to an approximate 45 mph ambient wind remote from the enclosure. Left view is a side view under zenith front wind, with deflections scaled 30,000:1. Right view is a front view under zenith side wind, scaled 50,000:1.

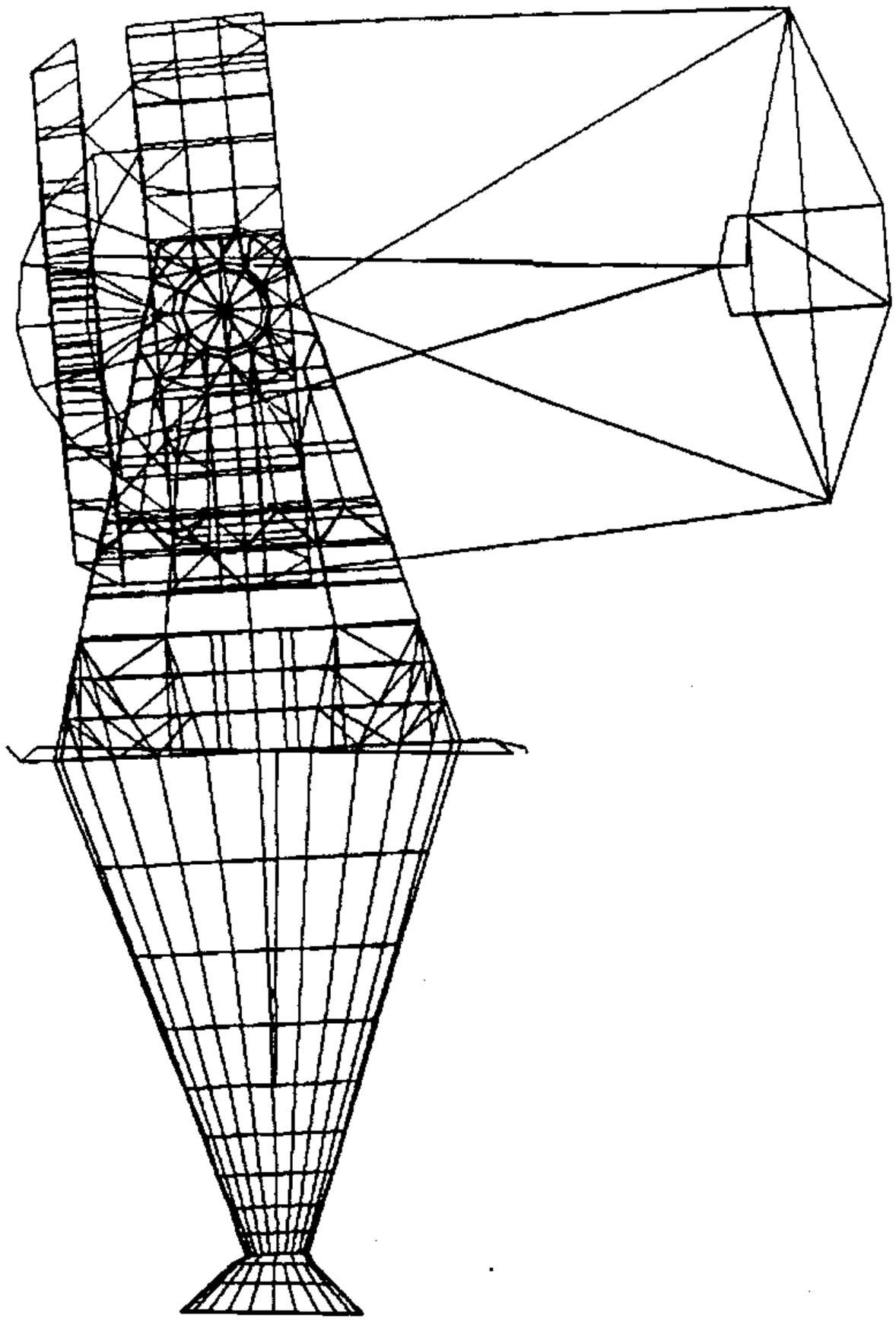

**FIGURE 22 -** Model WIYNTH - the complete telescope, horizon pointing. This side view shows the deflected shape of the system under front wind, scaled 50,000:1.

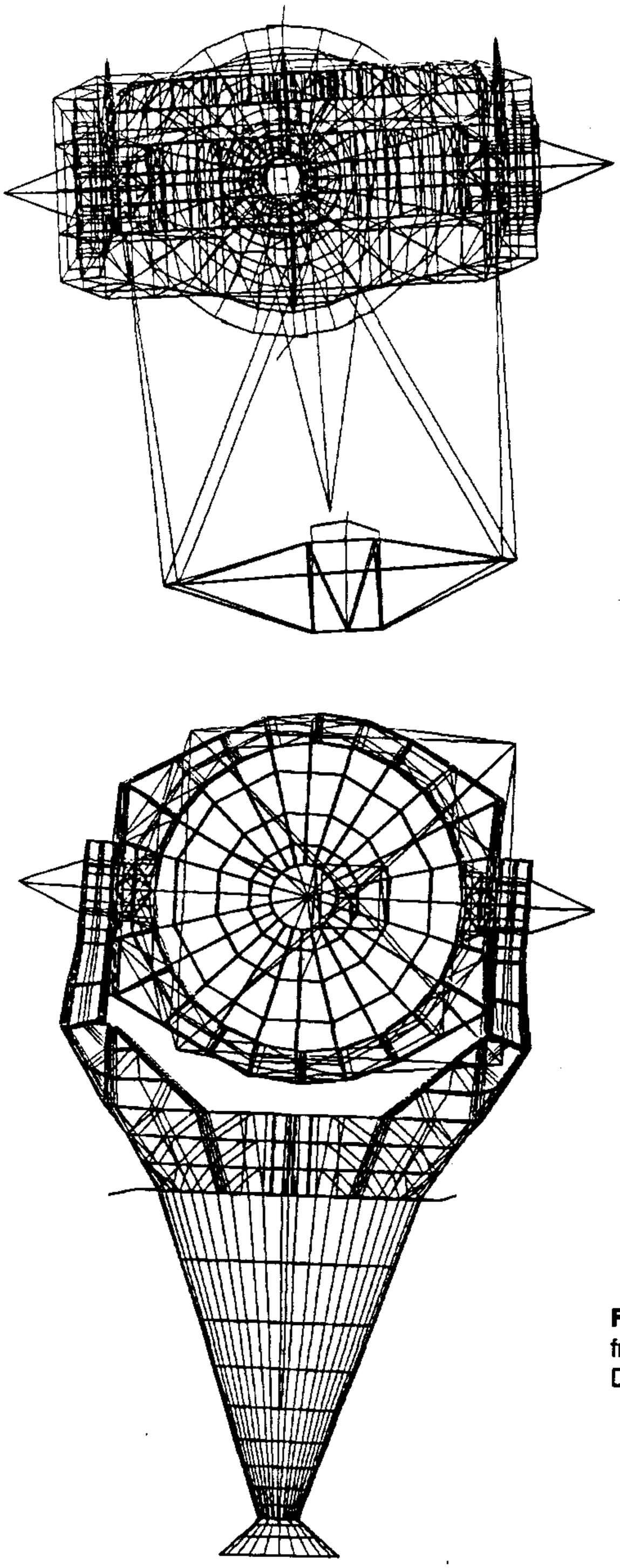

**FIGURE 23** - Model WIYNTH top and front views under horizon side wind. Deflections are scaled 50,000:1.

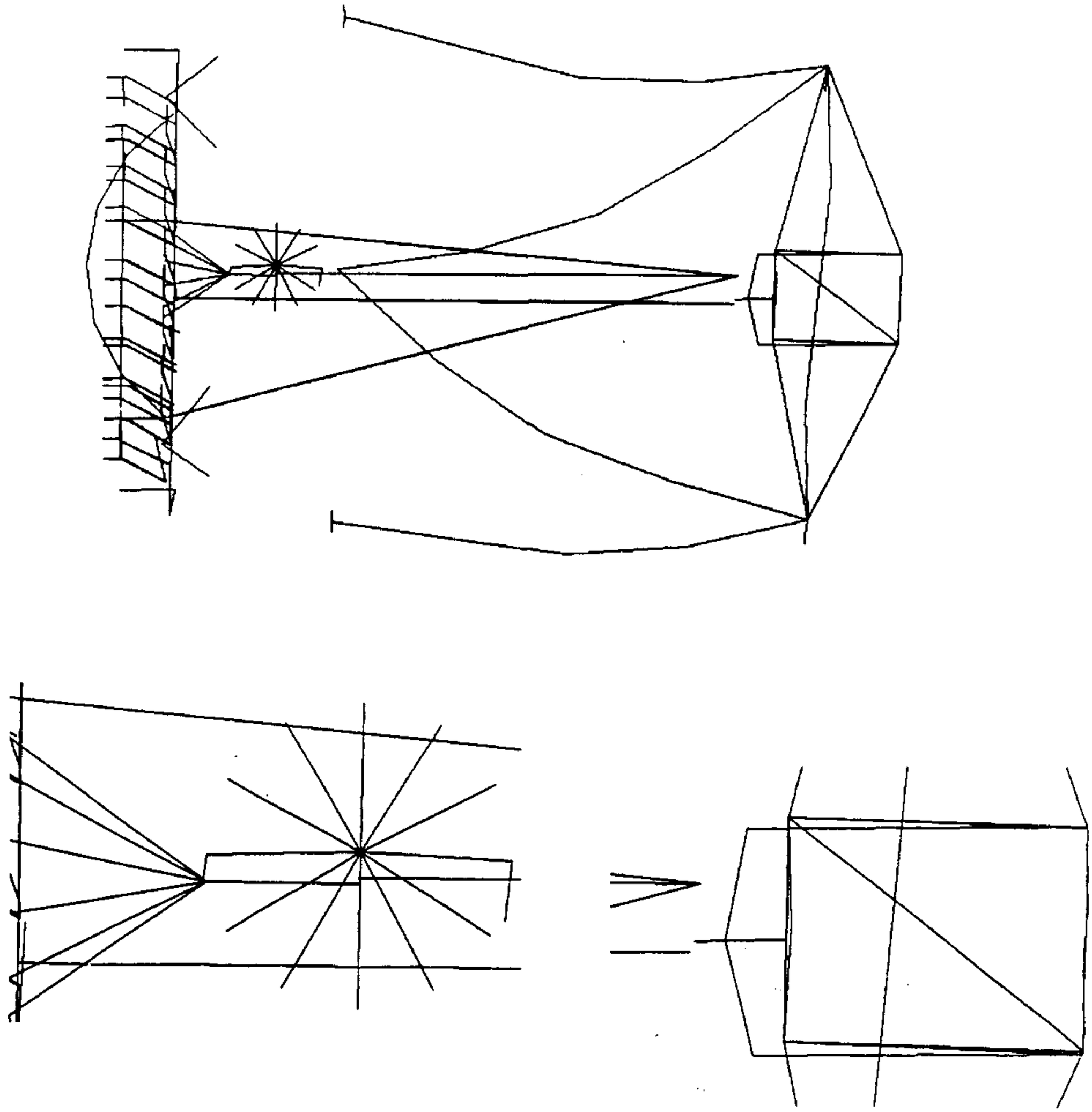

**FIGURE 24 -** Side view of model WINOSS1, load case 2, horizon gravity applied, scaled 500:1. Note from enlarged views the optical misalignments of the (two) primary mirror targets (with and without support system effects), and the secondary and tertiary mirror targets. PMT2 (the tripod target referenced directly to cell) also has a target reflected back at the altitude axis for easy determination of the motion of the axis of the primary relative to the altitude axis and tertiary. Absolute and relative displacements are summarized in the body of the report.

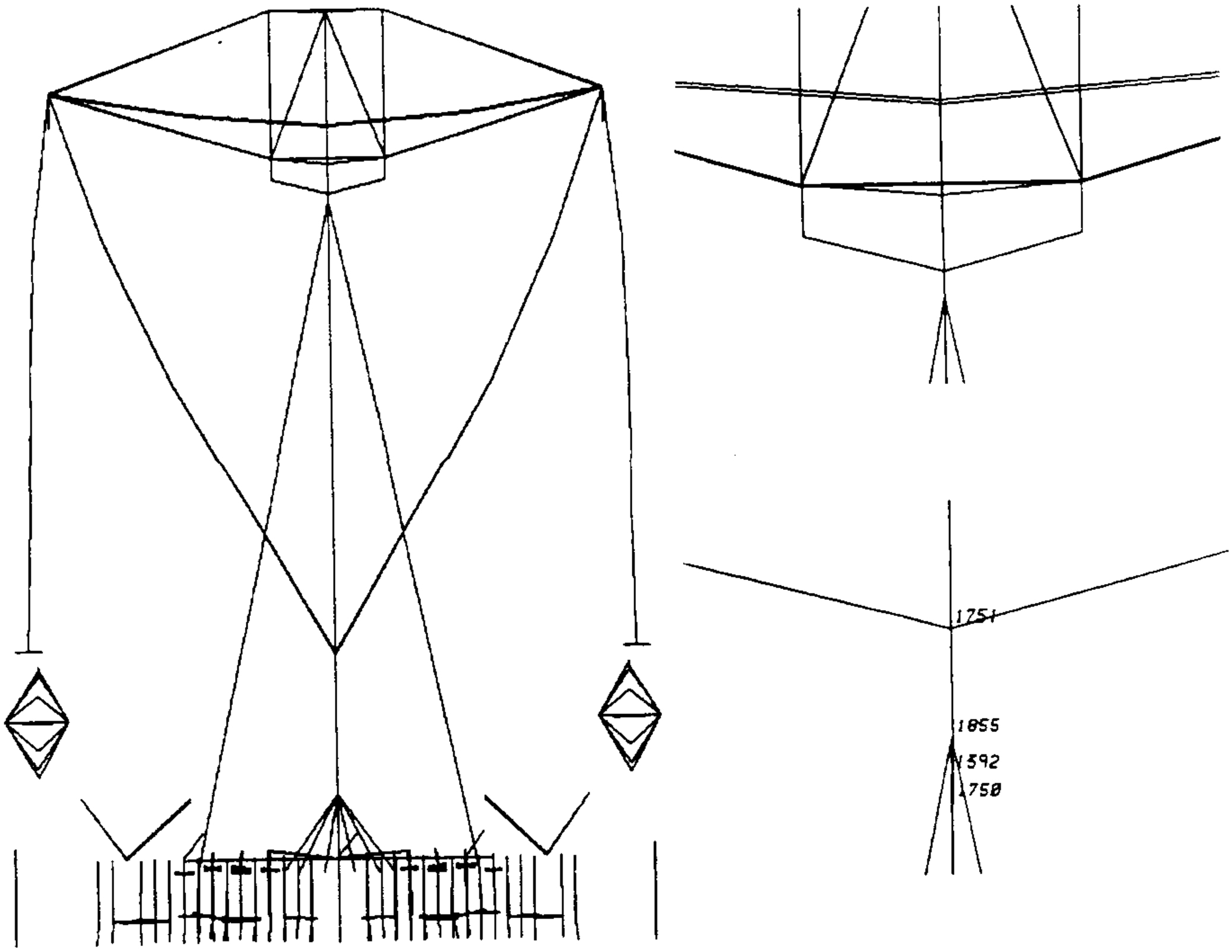


**FIGURE 25** - Front view of model WINOSS1, load case 1, zenith gravity applied, scaled 500:1. Note from the enlarged views the relative motion of the primary mirror targets (nodes 1392 and 1855) relative to the secondary mirror target, node 1750. Node 1751 is the center of gravity of the combined mirror and cell, modelled at 607 lbs.

# APPENDIX